

A coupled FE-BIE model for the static analysis of Timoshenko beams bonded to an orthotropic elastic half-plane

Enrico Tezzon^a, Nerio Tullini^a, Luca Lanzoni^b,

^a *Department of Engineering, University of Ferrara, Via Saragat 1, Ferrara, Italy*

e-mail: enrico.tezzon@unife.it; e-mail: nerio.tullini@unife.it

^b *Department of Engineering, University of Modena and Reggio Emilia, Via Vivarelli 10, Modena, Italy*

e-mail: luca.lanzoni@unimore.it

ABSTRACT

Interface displacements, surface tractions and stresses of a flexible beam bonded to an elastic orthotropic half-plane are analysed by means of a Finite Element-Boundary Integral Equation (FE-BIE) method. Numerical results are obtained by using locking-free shear deformable beams and piecewise constant interfacial reactions. Making use of the generalised Green's function for the half-plane, the mechanical behaviour of fully bonded or detached beams subjected to force, couple or thermal load is investigated. The special cases of a beam in bilateral frictionless contact with the half-plane and a beam having a vanishing bending rigidity (thin film) are considered also. In particular, the maximum bending moment of beams subjected to a vertical point force are compared with some closed-form solutions of the contact problem of a rigid indenter and with the solution of an infinite Euler-Bernoulli beam in bilateral frictionless contact with an isotropic substrate.

Keywords: Orthotropic half-plane, Euler-Bernoulli beam, Timoshenko beam, Mixed variational principle, Green function.

1 INTRODUCTION

The contact problem of bars, beams and plates bonded to an elastic support is an important issue that has generated much interest in recent years. It has been widely dealt with in areas of aerospace, electronic, marine, transportation and infrastructure. In the framework of civil engineering, this topic has been dealt with in order to study soil-structure interaction problems or to investigate the effect induced by some reinforcements to increase the load-bearing capacity of existing structural elements. The latter application has been considered in Fiber-Reinforced Polymer (FRP) strengthening of concrete, steel or timber structures [1, 2, 3].

The contact problem involved in the indentation of an elastic half-plane has been treated by many authors under the assumptions of frictionless or fully adhesive contact, see [4, 5, 6] and references cited therein. The solution of a line force acting onto an elastic half-space was usually the main tool to study the contact problem. In particular, limiting to orthotropic or transversely isotropic half-plane under normal and tangential loadings acting onto the half-plane boundary, references have to be made to [7-13].

Early studies concerning thin films welded to an elastic substrate adopted series approximation method to solve singular integral equations including proper Green's function, see [14, 15, 16] and references cited therein. Series approximation method was also used to study the bending problem of Euler-Bernoulli beams resting on an isotropic half-plane, under the assumptions of frictionless [17] or fully adhesive contact [18]. The influence of shear deformation was considered in [16, 19]. In particular, in [16] the bilateral frictionless contact between a transversely loaded Timoshenko beam and an elastic isotropic layer is analysed, whereas the unilateral frictionless contact between a shear deformable beam and an elastic layer supported by a rigid base is considered in [19].

The mechanical behaviour of single or multi-layered systems subjected to different loading conditions can be straightforwardly assessed by means of the Finite Element Method (FEM) due to its potential and versatility. Nonetheless, FEM undergoes important limitations when applied to

film-substrate systems [20]. Indeed, owing to the thinness of the layers typically involved in many thin film-based devices and coated systems, a refined mesh must be used, thus leading to a computer-time consuming. A proper grid refinement is needed in the neighbourhood of geometric discontinuities also in order to capture properly stress and strain localizations, whose knowledge is an important issue for many engineering tasks, ranging from the mechanical behaviour of MEMS and NEMS [21], to the analysis of the punch problem of coated systems prone to crack formations [22, 23]. Moreover, in order to simulate the half-plane, FE meshes should be extended to a region significantly greater than the contact area, with detrimental effect on the time needed to carry out the numerical simulations. Finally, it should be remarked that, by modelling the covers through beam elements and the underlying half-plane by means of classical two-dimensional FEs, the angular continuity between the cover and the substrate cannot be imposed exactly as the connection between the elements occurs at discrete points.

Boundary Element Method (BEM) is a particularly advantageous tool for reproducing the response of an elastic half-plane because only the substrate boundary has to be discretized, see [24] and references cited therein. However, substrate tractions are usually considered as nodal reactions in the FE model of the foundation beam and the rotation continuity between beam and substrate is neglected. Alternatively, BE technique can be used to evaluate the mechanical behaviour of coated systems involving thin layers, as long as the nearly-singular integrals existing in the BE formulations are handled correctly [25, 26]. Nonetheless, beam model can be computationally more efficient than thin layer.

Otherwise, the behaviour of the soil can be approximated by incorporating a proper model for the substrate. As an example, Cheung and Zienkiewicz [27], and Cheung and Nag [28] performed a numerical model in which the deflection of the foundation and, in turn, the corresponding flexibility matrix, involve the fundamental Boussinesq's solution for the elastic half-plane, thus simulating accurately the interaction between loaded beams and plates in contact with an elastic support. However, based on such an approach, the continuity of the slope between the beam and the half-

plane boundary cannot be imposed. Indeed, the connection among the beam and the substrate elements is realized by means of a finite number of pinned-clamped rigid links acting at equally spaced points, thus enforcing the continuity of the transversal deflection only. Moreover, the inversion of the substrate flexibility matrix is needed, thus consuming high computer-time.

In the present paper, a static analysis of beams in plane strain or plane stress condition bonded to a homogeneous, linearly elastic and orthotropic half-plane, with a plane of elastic symmetry parallel to the boundary, is performed by using a coupled Finite Element-Boundary Integral Equation (FE-BIE) model. The proposed approach involves the Green's function for the half-plane, thus providing a proper relation between the displacement and the interfacial stress fields at the substrate boundary, whereas a standard displacement-based formulation is used for the beam. The mechanical response of the half-plane is represented through a weakly singular integral equation, which solution is given analytically, thus avoiding singular and hyper-singular integrals typically involved in the classical BEM formulation. The independent unknowns of the problem are the displacement and the stress fields at the interface. It is worth noting that only the beam in contact with the substrate boundary has to be discretized. Unlike the numerical analyses available in the literature (e.g. [27, 28]), the proposed approach enforces the angular continuity between the foundation beam and the half-plane boundary at the node locations. Conversely to the classical FEM-BEM formulations, only symmetric soil matrices are involved in the proposed method, thus avoiding the computational cost due to the lack of symmetry of the BEM coefficient matrix. Note also that, differently to the standard FEM approaches in which a refined mesh requires a stiffness matrix with dimensions that are several times the square of the number of FEs used for the foundation beam, in the present model the resolving matrix has dimensions proportional to the number of the foundation beam FEs. This makes it possible to obtain very accurate solutions with low computational cost, as shown in [29], where a static analysis of both Euler-Bernoulli and Timoshenko beams bonded to an isotropic half-plane has been performed founding an excellent convergence rate as compared with those of other standard numerical methods.

Once the unknowns have been determined, the internal forces on the beam are determined through usual post-processing analysis. Recently, the static analysis of Timoshenko beams in frictionless [30] or fully adhesive contact [29] with an isotropic half-plane has been performed based on a similar mixed formulation (an analogous study concerning bars and thin coatings can be found in [31]). Furthermore, the FE-BIE coupling method has been also used to study the buckling of Euler-Bernoulli [32] and Timoshenko [33] beams in bilateral frictionless contact with an elastic support. The proposed approach can be straightforwardly extended to investigate the buckling of homogeneous or graded layers welded to an elastic substrate, with particular reference to the instability analysis of thermal barrier coatings, by following the approach adopted in [32, 33]. However, for such elements, wrinkle instabilities can occur, particularly in stiff coatings bonded to compliant substrates under compressive loads [34]. Therefore, a proper mesh refinement of the coating is mandatory in order to capture properly the wrinkle wavelength.

Numerical examples of FRP laminate bonded to wood substrate and concrete foundation resting on soil are treated by assuming beam or membrane theory for the stiffener and, concerning the contact condition, perfect adhesion or bilateral frictionless contact. Beams with different bending rigidity, loaded by a vertical point force at the midspan are considered in plane strain state firstly. The maximum value achieved by the bending moment is investigated and compared with analytic solution present in the literature. Moreover, a detached and fully bonded beam subjected to a vertical point force at one end are analysed. Afterwards, beams subjected to horizontal force or thermal variation under plane stress assumption are investigated. It is shown that the shear force at the beam ends can be significantly affected by shear deformation according to the Timoshenko beam theory. Finally, a shallow foundation loaded by a moment at the midspan is studied as a Timoshenko beam in perfect adhesion as well as in bilateral frictionless contact with an elastic soil.

2 VARIATIONAL FORMULATION

A shear deformable beam with length L , height h and width b , bonded to an orthotropic semi-infinite substrate in a generalized plane stress or plane strain state is considered here. Reference is made to a Cartesian coordinate system $(O; x, z)$ having the x axis coincident with the centroidal axis of the beam and the z axis is downward directed (Fig. 1). Distributed horizontal and vertical external loads $p_x(x)$, $p_z(x)$, couple $m(x)$ as well as thermal variation $\Delta T(x)$ act along the beam. The beam is supposed in perfect adhesion with the half-plane. According to this assumption, both interfacial shear and normal tractions, $r_x(x)$ and $r_z(x)$, will occur within the contact region.

Here, a mixed variational principle is used to study the beam-substrate system, including the Green's function for the orthotropic half-plane. The total potential energy of the system Π is given by adding the total potential energy of the beam Π_{beam} to that of the substrate Π_{soil} , i.e., $\Pi = \Pi_{\text{beam}} + \Pi_{\text{soil}}$. As limit cases, an inextensible thin coating with a vanishing bending rigidity bonded to a half-plane and a beam in bilateral frictionless contact with a half-plane are considered in some detail.

2.1 Total potential energy for the foundation beam

Assuming positive cross-section rotations φ in counter-clockwise direction, the horizontal and vertical components of the displacement field of the Timoshenko beam can be written as

$$u_{bx}(x, z) = u_{bx,0}(x) + \varphi(x) z, \quad u_{bz}(x, z) = u_z(x), \quad (1a,b)$$

where $u_{bx,0}$ is the axial displacement of the centroidal beam axis and u_z is the vertical displacement of both the beam and the half-plane boundary. The horizontal displacement of the lower side of the beam in contact with the half-plane boundary is given by $u_x(x) = u_{bx,0}(x) + \varphi(x) h/2$. The corresponding axial and shear strains are

$$\varepsilon_b = u'_{bx,0} + \varphi' z, \quad \gamma_b = u'_z + \varphi, \quad (2a,b)$$

where prime represents differentiation with respect to variable x . Plane state assumption yields the following stress-strain relations:

$$\sigma_b = E_0 \varepsilon_b, \quad \tau_b = G_b \gamma_b, \quad (3a,b)$$

where $E_0 = E_{x,b}$ or $E_0 = E_{x,b}/(1-\nu_{xy,b}\nu_{yx,b})$ for generalised plane stress or plane strain state respectively, $E_{x,b}$ is the Young's modulus of the beam along the x -axis, $\nu_{ij,b}$ is the Poisson's coefficient of the beam associated with the pair directions $i, j = x, y, z$, G_b is the shear modulus $G_{xz,b}$ of the beam.

The elastic strain energy of the beam, U_{beam} , can be written as the sum of the axial strain energy $U_{\text{beam},a}$ and the bending-transverse shear strain energy $U_{\text{beam},b}$. By using the strain components (2) and the stress-strain relations (3), the elastic strain energies $U_{\text{beam},a}$ and $U_{\text{beam},b}$ can be written as:

$$U_{\text{beam},a} = \frac{1}{2} \int_L E_0 A_b (u'_{bx,0} - \alpha_0 \Delta T)^2 dx, \quad (4a)$$

$$U_{\text{beam},b} = \frac{1}{2} \int_L [D_b (\varphi')^2 + k_b G_b A_b (u'_z + \varphi)^2] dx, \quad (4b)$$

where $A_b = bh$, $D_b = E_0 bh^3/12$ are the area and the flexural rigidity of the beam cross section, respectively, α_0 is the coefficient of thermal expansion of the beam, k_b is the shear correction factor [35, 36]

$$k_b = \frac{5}{6 - \nu_{xz,b} G_b / E_{x,b}}, \quad k_b = \frac{5}{6 - (\nu_{xz,b} + \nu_{xy,b} \nu_{yz,b}) G_b / E_{x,b}}, \quad (5)$$

for a plane stress or a plane strain state, respectively.

Finally, the total potential energy of the beam, Π_{beam} , is assessed by adding the axial part $\Pi_{\text{beam},a}$ to the bending component $\Pi_{\text{beam},b}$, which are obtained from the strain energy contributions and the potential energy of the external loads, resulting in

$$\Pi_{\text{beam},a} = U_{\text{beam},a} - b \int_L (p_x - r_x) u_{bx,0} dx, \quad (6a)$$

$$\Pi_{\text{beam},b} = U_{\text{beam},b} - b \int_L [(p_z - r_z) u_z + (m - r_x h/2) \varphi] dx. \quad (6b)$$

2.2 Total potential energy for the orthotropic substrate

According to Voigt compact notation [6], the stress-strain relationship of a linearly elastic material can be expressed by the Hooke's law $\boldsymbol{\varepsilon} = \mathbf{S} \boldsymbol{\sigma}$, where the compliance matrix \mathbf{S} can be written making reference to the canonical base (O; x, z). As known, for an orthotropic body exhibiting three perpendicular planes of elastic symmetry xz , yz , and xz in a plane state, the strain-stress relationship reduces to

$$\begin{bmatrix} \varepsilon_{xx} \\ \varepsilon_{zz} \\ 2\varepsilon_{xz} \end{bmatrix} = \begin{bmatrix} R_{11} & R_{13} & 0 \\ R_{13} & R_{33} & 0 \\ 0 & 0 & R_{55} \end{bmatrix} \begin{bmatrix} \sigma_{xx} \\ \sigma_{zz} \\ \sigma_{xz} \end{bmatrix}, \quad (7)$$

where the elastic compliance constants involved in Eq. (7) can be written as

$$R_{11} = \frac{1}{E_x}, \quad R_{33} = \frac{1}{E_z}, \quad R_{13} = -\frac{\nu_{xz}}{E_x} = -\frac{\nu_{zx}}{E_z}, \quad R_{55} = \frac{1}{G_{xz}}, \quad (8a,b,c,d)$$

$$R_{11} = \frac{1 - \nu_{xy} \nu_{yx}}{E_x}, \quad R_{33} = \frac{1 - \nu_{zy} \nu_{yz}}{E_z}, \quad R_{13} = -\frac{\nu_{xz} + \nu_{xy} \nu_{yz}}{E_x} = -\frac{\nu_{zx} + \nu_{yx} \nu_{zy}}{E_z}, \quad R_{55} = \frac{1}{G_{xz}}, \quad (9a,b,c,d)$$

for plane stress state, Eq. (8), or plane strain state, Eq. (9), respectively, where E_i denotes the Young's modulus along the directions $i = x, z$, G_{ij} and ν_{ij} are the shear modulus and Poisson's coefficient, respectively, associated with the pair directions $i, j = x, y, z$. In particular, due to this special kind of material symmetry, $\nu_{ij}/E_i = \nu_{ji}/E_j$.

In the following, three combinations of the elastic compliance constants are used

$$c_1 = \left(\frac{R_{11}}{R_{33}} \right)^{1/4}, \quad c_2 = \left(2 + \frac{R_{55} + 2R_{13}}{\sqrt{R_{11}R_{33}}} \right)^{1/2}, \quad c_3 = \left(\frac{R_{11}}{R_{33}} \right)^{1/2} + \frac{R_{13}}{R_{33}}. \quad (10a,b,c)$$

In particular, in plane stress state, making use of Eq. (8), Eq. (10) reduces to

$$c_1 = \left(\frac{E_z}{E_x} \right)^{1/4}, \quad c_2 = \left(2 + \frac{\sqrt{E_x E_z}}{G_{xz}} - 2\nu_{xz} \left(\frac{E_z}{E_x} \right)^{1/2} \right)^{1/2}, \quad c_3 = \left(\frac{E_z}{E_x} \right)^{1/2} - \nu_{zx}, \quad (11a,b,c)$$

while in plane strain state, by substituting Eq. (9) into Eq. (10), the constants c_1 , c_2 , c_3 become

$$c_1 = \left(\frac{E_z}{E_x} \frac{1 - \nu_{xy}\nu_{yx}}{1 - \nu_{zy}\nu_{yz}} \right)^{1/4}, \quad c_2 = \left(2 + \sqrt{\frac{E_z}{(1 - \nu_{xy}\nu_{yx})(1 - \nu_{zy}\nu_{yz})}} \left(\frac{\sqrt{E_x}}{G_{xz}} - \frac{2(\nu_{xz} + \nu_{xy}\nu_{yz})}{\sqrt{E_x}} \right) \right)^{1/2}, \quad (12a,b)$$

$$c_3 = \left(\frac{E_z}{E_x} \frac{1 - \nu_{xy}\nu_{yx}}{1 - \nu_{zy}\nu_{yz}} \right)^{1/2} - \frac{\nu_{zx} + \nu_{yx}\nu_{zy}}{1 - \nu_{zy}\nu_{yz}}. \quad (12c)$$

It is worth remarking that, for an isotropic substrate, the elastic compliance component R_{33} of the half-plane in z -direction is equal to $1/E$ and the substrate coefficients are $c_1 = 1$, $c_2 = 2$, $c_3 = c$, where $E = E_{\text{soil}}$ and $c = 1 - \nu_{\text{soil}}$ or $E = E_{\text{soil}}/(1 - \nu_{\text{soil}}^2)$ and $c = (1 - 2\nu_{\text{soil}})/(1 - \nu_{\text{soil}})$ for a generalized plane stress or plane strain state, respectively, E_{soil} and ν_{soil} being the Young's modulus and Poisson ratio of the isotropic substrate.

The solutions to the two-dimensional problem for a homogeneous, linear elastic and orthotropic half-plane loaded by a point force normal or tangential to its boundary are given in [12, 13]. In particular, the surface displacement $u_i(x)$, with $i = x, z$, due to a point force $P_i(\hat{x})$ applied to the half-plane boundary, can be expressed in closed form as $u_i(x) = g(x, \hat{x}) P_i(\hat{x})$, where the Green's function $g(x, \hat{x})$ is given by the following expression:

$$g(x, \hat{x}) = -\frac{c_1 c_2 R_{33}}{\pi} \ln \frac{|x - \hat{x}|}{d}, \quad (13)$$

being d an arbitrary length related to a rigid-body displacement.

After some cumbersome algebraic manipulation of the results reported in [12, 13], the horizontal and vertical displacements of a point of the orthotropic half-plane boundary due to the combined action of tangential and normal tractions can be written as:

$$u_x(x) = c_1^2 \int_L g(x, \hat{x}) r_x(\hat{x}) d\hat{x} - \frac{c_3}{2} R_{33} \left[\int_{x_0}^x r_z(\hat{x}) d\hat{x} - \int_x^{x_L} r_z(\hat{x}) d\hat{x} \right], \quad (14a)$$

$$u_z(x) = \int_L g(x, \hat{x}) r_z(\hat{x}) d\hat{x} + \frac{c_3}{2} R_{33} \left[\int_{x_0}^x r_x(\hat{x}) d\hat{x} - \int_x^{x_L} r_x(\hat{x}) d\hat{x} \right], \quad \text{with } x_0 < x < x_L, \quad (14b)$$

where x_0, x_L are the abscissas of the beam ends. Therefore, a combination of only four elastic constants characterises the displacement field (14).

Making use of the theorem of work and energy for exterior domains [37], it can be shown that the total potential energy Π_{soil} for the half-plane equals one half of the work of external loads [30, 31, 29], i.e.,

$$\Pi_{\text{soil}} = -\frac{b}{2} \int_L (r_x u_x + r_z u_z) dx. \quad (15)$$

Substituting Eq. (14) into Eq. (15) yields $\Pi_{\text{soil}} = \Pi_{\text{soil},a} + \Pi_{\text{soil},b}$, where

$$\Pi_{\text{soil},a} = -\frac{b}{2} \int_L r_x(x) dx \left\{ c_1^2 \int_L g(x, \hat{x}) r_x(\hat{x}) d\hat{x} - \frac{c_3}{2} R_{33} \left[\int_{x_0}^x r_z(\hat{x}) d\hat{x} - \int_x^{x_L} r_z(\hat{x}) d\hat{x} \right] \right\}, \quad (16a)$$

$$\Pi_{\text{soil},b} = -\frac{b}{2} \int_L r_z(x) dx \left\{ \int_L g(x, \hat{x}) r_z(\hat{x}) d\hat{x} + \frac{c_3}{2} R_{33} \left[\int_{x_0}^x r_x(\hat{x}) d\hat{x} - \int_x^{x_L} r_x(\hat{x}) d\hat{x} \right] \right\}. \quad (16b)$$

2.3 Total potential energy for the beam-substrate system

The total potential energy of the beam-substrate system $\Pi = \Pi_{\text{beam}} + \Pi_{\text{soil}}$ is a mixed variational formulation with variational functions represented by displacements $u_{bx,0}, u_z$ and rotation φ , as well

as interfacial shear and normal tractions r_x and r_z along the contact region. It is worth noting that using Green's function given by Eq. (13) reduces the domain of integration to the beam length only. For an isotropic substrate, the total potential energy Π reduces to that reported in [29].

Several particular cases derive from the proposed mixed variational formulation. For instance, a beam in bilateral frictionless contact with the underlying substrate involves null interfacial shear tractions r_x along the contact region. Accordingly, the displacement field provided by Eq. (14) reads

$$u_x(x) = -\frac{c_3}{2} R_{33} \left[\int_{x_0}^x r_z(\hat{x}) d\hat{x} - \int_x^{x_L} r_z(\hat{x}) d\hat{x} \right], \quad (17a)$$

$$u_z(x) = \int_L g(x, \hat{x}) r_z(\hat{x}) d\hat{x}, \quad (17b)$$

and, accordingly, the total potential energy of orthotropic half-plane Π_{soil} becomes

$$\Pi_{\text{soil}} = \Pi_{\text{soil,b}} = -\frac{b}{2} \int_L r_z u_z dx = -\frac{b}{2} \int_L r_z(x) dx \int_L g(x, \hat{x}) r_z(\hat{x}) d\hat{x}. \quad (18)$$

The displacement field (17) is similar to Eq. (12) reported in [30], where a beam in bilateral frictionless contact with an isotropic substrate is considered, except for different values of the Young's modulus and the coefficient c . Therefore, an orthotropic substrate behaves like an isotropic soil having an equivalent Young's modulus $E = 2/(c_1 c_2 R_{33})$ and a ratio $c/E = c_3 R_{33}$, with $c = 2 c_3/(c_1 c_2)$. Thus, the FE-BIE methods as well as the results shown in [30] can be used. In particular, in the case of a rigid punch resting on an orthotropic half-plane, the normal tractions under the punch are the same of those found for the indentation problem of an isotropic half-plane [6]. However, the stress and displacement fields in the half-plane will differ from those found in the case of isotropy.

A beam with a small bending rigidity may be considered as a thin coating where the normal tractions r_z can be neglected. Then, the displacement field (14) reduces to

$$u_x(x) = c_1^2 \int_L g(x, \hat{x}) r_x(\hat{x}) d\hat{x}, \quad (19a)$$

$$u_z(x) = \frac{c_3}{2} R_{33} \left[\int_{x_0}^x r_x(\hat{x}) d\hat{x} - \int_x^{x_L} r_x(\hat{x}) d\hat{x} \right], \quad (19b)$$

and the total potential (15) becomes

$$\Pi_{\text{soil}} = \Pi_{\text{soil,a}} = -\frac{b}{2} \int_L r_x u_x dx = -\frac{b}{2} c_1^2 \int_L r_x(x) dx \int_L g(x, \hat{x}) r_x(\hat{x}) d\hat{x}. \quad (20)$$

The displacement field (19) is similar to Eq. (13) reported in [31], where a thin coating bonded to an isotropic substrate is studied, except for different values of the Young's modulus and the coefficient c . Therefore, an orthotropic substrate behaves like an isotropic soil having an equivalent Young's modulus $E = 2/(c_1^3 c_2 R_{33}) = 2 c_1/(c_2 R_{11})$ and a ratio $c/E = c_3 R_{33}$, with $c = 2 c_3/(c_1^3 c_2)$. Therefore, the analyses made in [31] can be employed. In particular, in the case of an inextensible stiffener bonded to an orthotropic half-plane, the interfacial shear tractions r_x are the same of those founded for an isotropic half-plane.

3 FINITE ELEMENT MODEL

Both the foundation beam and the substrate boundary are subdivided into FEs sharing the same mesh. Nevertheless, the mesh of the beam could be chosen independently from that used for the half-plane boundary. The generic i th FE has a length $l_i = |x_{i+1} - x_i|$ where x_i and x_{i+1} are the initial and end coordinates. Assuming a dimensionless local coordinate $\xi = x/l_i$, the displacements of the centroidal axis of beam can be approximated as

$$u(\xi) = \mathbf{N}_a(\xi) \mathbf{u}_{xi}, \quad [v(\xi), \varphi(\xi)]^T = \mathbf{N}_b(\xi) \mathbf{q}_{zi}, \quad (21a,b)$$

where $\mathbf{u}_{xi} = [u_{x,i}, u_{x,i+1}]^T$ and $\mathbf{q}_{zi} = [u_{z,i}, \varphi_i, u_{z,i+1}, \varphi_{i+1}]^T$ are the vectors of nodal displacements, while $\mathbf{N}_a(\xi) = [N_{a,1}, N_{a,2}]$ is the vector collecting the linear Lagrangian functions, $N_{a,1} = 1 - \xi$ and $N_{a,2} = \xi$, whereas $\mathbf{N}_b(\xi)$ is the matrix of the “modified” Hermitian shape functions [29, 30, 38, 39]:

$$N_{b,11} = [1 - 3\xi^2 + 2\xi^3 + \phi_i(1 - \xi)]/(1 + \phi_i), \quad N_{b,12} = -l_i \xi [(1 - \xi)^2 + \phi_i(1 - \xi)/2]/(1 + \phi_i), \quad (22a, b)$$

$$N_{b,13} = [3\xi^2 - 2\xi^3 + \phi_i\xi]/(1 + \phi_i), \quad N_{b,14} = -l_i \xi [-\xi + \xi^2 - \phi_i(1 - \xi)/2]/(1 + \phi_i), \quad (22c, d)$$

$$N_{b,21} = 6\xi(1 - \xi)/[l_i(1 + \phi_i)], \quad N_{b,22} = [1 - 4\xi + 3\xi^2 + \phi_i(1 - \xi)]/(1 + \phi_i), \quad (22e, f)$$

$$N_{b,23} = -6\xi(1 - \xi)/[l_i(1 + \phi_i)], \quad N_{b,24} = (-2\xi + 3\xi^2 + \phi_i\xi)/(1 + \phi_i), \quad (22g, h)$$

being $\phi_i = 12D_b/(k_b G_b A_b l_i^2)$ dimensionless coefficients accounting for the shear deformation according to the Timoshenko beam theory. As shown in [40], the finite element interpolation functions (22) gives exact nodal displacements as they derive from the exact solution of the homogeneous governing equations for a Timoshenko beam. Moreover, Eqs. (22) reduce to the classical Hermitian polynomials (and to their derivatives) when shear deformations are negligible, so resulting in locking-free FEs [40, 41].

The tractions may be approximated as

$$r_x(\xi) = [\boldsymbol{\rho}(\xi)]^T \mathbf{r}_{xi}, \quad r_z(\xi) = [\boldsymbol{\rho}(\xi)]^T \mathbf{r}_{zi}, \quad (23a,b)$$

where \mathbf{r}_{xi} , \mathbf{r}_{zi} denote nodal interfacial shear and normal tractions, respectively, and vector $\boldsymbol{\rho}$ collects constant shape functions, i.e., only piecewise constant functions are used to interpolate \mathbf{r}_x and \mathbf{r}_z and $\boldsymbol{\rho}(\xi)$ is assumed to be unitary along the generic FE.

Substituting Eqs. (21) and (23) into the total potential energy of the beam-substrate system Π and assembling over all elements, the potential energy turns out to be

$$\begin{aligned} \Pi(\mathbf{u}_x, \mathbf{q}_z, \mathbf{r}_x, \mathbf{r}_z) = & \frac{1}{2} \mathbf{u}_x^T \mathbf{K}_a \mathbf{u}_x + \frac{1}{2} \mathbf{q}_z^T \mathbf{K}_b \mathbf{q}_z - \mathbf{u}_x^T \mathbf{f}_x - \mathbf{q}_z^T \mathbf{f}_z + \mathbf{u}_x^T \mathbf{H}_{xx} \mathbf{r}_x + \mathbf{q}_z^T \mathbf{H}_{zz} \mathbf{r}_z + \mathbf{q}_z^T \mathbf{H}_{zx} \mathbf{r}_x \\ & - \frac{1}{2} \mathbf{r}_x^T \mathbf{G}_{xx} \mathbf{r}_x - \frac{1}{2} \mathbf{r}_z^T \mathbf{G}_{zz} \mathbf{r}_z - \frac{1}{2} \mathbf{r}_x^T \mathbf{G}_{xz} \mathbf{r}_z - \frac{1}{2} \mathbf{r}_z^T \mathbf{G}_{zx} \mathbf{r}_x, \end{aligned} \quad (24)$$

where $\mathbf{K}_a, \mathbf{K}_b$ are the beam stiffness matrices and $\mathbf{f}_x, \mathbf{f}_z$ denote the external load vectors, whose components for the i th FE can be written in the usual form:

$$k_{a,ij} = \frac{1}{l_i} \int_0^1 E_0 A_b(\xi) N'_{a,i}(\xi) N'_{a,j}(\xi) d\xi, \quad (25a)$$

$$k_{b,ij} = \frac{1}{l_i} \int_0^1 D_b(\xi) \left[N'_{b,2i}(\xi) N'_{b,2j}(\xi) + \frac{12}{\phi_i} \left(\frac{1}{l_i} N'_{b,1i}(\xi) + N_{b,2i}(\xi) \right) \left(\frac{1}{l_i} N'_{b,1j}(\xi) + N_{b,2j}(\xi) \right) \right] d\xi, \quad (25b)$$

$$f_{x,i} = \int_0^1 \left(N_{a,i}(\xi) p_x(\xi) b l_i + N'_{a,i}(\xi) E_0 A(\xi) \alpha_b \Delta T \right) d\xi, \quad (26a)$$

$$f_{z,i} = b l_i \int_0^1 \left(N_{b,1i}(\xi) p_z(\xi) + N_{b,2i}(\xi) m(\xi) \right) d\xi. \quad (26b)$$

The components of matrices $\mathbf{H}_{xx}, \mathbf{H}_{zz}, \mathbf{H}_{xz}$ appearing in Eq. (22) descend by the potential energy of the substrate tractions appearing in Eqs. (6a, b) and play a key role as they enforce the compatibility of displacements and rotations between the beam and the substrate. The following expressions hold for the generic FE:

$$h_{xx,ij} = b l_i \int_0^1 N_{a,i}(\xi) \rho_{a,j}(\xi) d\xi, \quad (27a)$$

$$h_{zz,ij} = b l_i \int_0^1 N_{b,1i}(\xi) \rho_{b,j}(\xi) d\xi, \quad (27b)$$

$$h_{xz,ij} = \frac{b h l_i}{2} \int_0^1 N_{b,2i}(\xi) \rho_{a,j}(\xi) d\xi. \quad (27c)$$

Note that expressions (27) coincide with Eqs. (25) reported in [29].

Note also that matrices \mathbf{G}_{xx} , \mathbf{G}_{zz} , \mathbf{G}_{xz} , \mathbf{G}_{zx} are fully populated since they account for the nonlocal relation between beam displacements and surface tractions. These matrices can be grouped in the following substrate matrix

$$\mathbf{G} = -bR_{33}\tilde{\mathbf{G}} = -bR_{33}\begin{bmatrix} c_1^2 \tilde{\mathbf{G}}_{xx} & c_3 \tilde{\mathbf{G}}_{xz} \\ c_3 \tilde{\mathbf{G}}_{xz}^T & \tilde{\mathbf{G}}_{zz} \end{bmatrix}. \quad (28)$$

The components of the matrix \mathbf{G} are given by:

$$\tilde{g}_{xx,ij} = \tilde{g}_{zz,ij} = \frac{c_1 c_2}{\pi} \int_{x_i}^{x_{i+1}} \rho_i(x) dx \int_{x_j}^{x_{j+1}} \ln|x - \hat{x}| \rho_j(\hat{x}) d\hat{x}, \quad (29a)$$

$$\tilde{g}_{xz,ij} = \int_{x_i}^{x_{i+1}} \rho_i(x) dx \left[\int_{x_0}^x \rho_j(\hat{x}) d\hat{x} - \int_x^{x_L} \rho_j(\hat{x}) d\hat{x} \right], \quad (29b)$$

where the contribution due to the arbitrary length d has been omitted since rigid-body displacements can be imposed in post-processing analysis. For instance, both the horizontal and vertical displacements at one beam end or at the beam midspan can be set to zero. The integral in Eq. (29a) is weakly singular, i.e. it always exists and it is finite. Substituting piecewise constant functions (23) in Eq. (29a), analytical integration yields

$$\tilde{g}_{xx,ii} = \tilde{g}_{zz,ii} = \frac{c_1 c_2}{\pi} l_i^2 \left(\frac{3}{2} - \ln l_i \right), \quad (30a)$$

$$\tilde{g}_{xx,ij} = \tilde{g}_{zz,ij} = \frac{c_1 c_2}{\pi} \left[\frac{3}{2} l_i l_j + G(x_{j+1} - x_{i+1}) - G(x_{j+1} - x_i) - G(x_j - x_{i+1}) + G(x_j - x_i) \right] \text{ for } i \neq j, \quad (30b)$$

with $G(x) = x^2/2 \ln|x|$, whereas the components of matrix $\tilde{\mathbf{G}}_{xz}$, Eq. (29b), are the following

$$\tilde{g}_{xz} = \begin{cases} \tilde{g}_{xz,ij} = -l_i l_j / 2 & \text{if } i > j \\ \tilde{g}_{xz,ii} = 0 & \text{if } i = j \\ \tilde{g}_{xz,ij} = l_i l_j / 2 & \text{if } i < j \end{cases}. \quad (31)$$

For an isotropic half-plane, matrix (28) reduces to Eq. (42c) reported in [29].

Requiring the stationarity of the potential energy (24), the following system of equations governing the response of the beam-substrate system is obtained:

$$\begin{bmatrix} \mathbf{K} & \mathbf{H} \\ \mathbf{H}^T & -\mathbf{G} \end{bmatrix} \begin{Bmatrix} \mathbf{q} \\ \mathbf{r} \end{Bmatrix} = \begin{Bmatrix} \mathbf{f} \\ \mathbf{0} \end{Bmatrix}. \quad (32)$$

where

$$\mathbf{K} = \begin{bmatrix} \mathbf{K}_a & \mathbf{0} \\ \mathbf{0} & \mathbf{K}_b \end{bmatrix}, \quad \mathbf{H} = \begin{bmatrix} \mathbf{H}_{xx} & \mathbf{0} \\ \mathbf{H}_{xz} & \mathbf{H}_{zz} \end{bmatrix}, \quad (33a, b)$$

$$\mathbf{q} = \begin{bmatrix} \mathbf{u}_x \\ \mathbf{q}_z \end{bmatrix}, \quad \mathbf{r} = \begin{bmatrix} \mathbf{r}_x \\ \mathbf{r}_z \end{bmatrix}, \quad \mathbf{f} = \begin{bmatrix} \mathbf{f}_x \\ \mathbf{f}_z \end{bmatrix}. \quad (34a,b,c)$$

For the sake of completeness, classical results referred to a prismatic beam subjected to distributions of loads $p_x(x)$, $p_z(x)$, couple $m(x)$ as well as thermal variation ΔT are recalled. The system of equations (32) concerning a prismatic beam bonded to an orthotropic half-plane can be written in dimensionless form as

$$\begin{bmatrix} D_b/L^3 \tilde{\mathbf{K}} & b\tilde{\mathbf{H}} \\ b\tilde{\mathbf{H}}^T & -bR_{33}\tilde{\mathbf{G}} \end{bmatrix} \begin{Bmatrix} \mathbf{q} \\ \mathbf{r} \end{Bmatrix} = \begin{Bmatrix} b\tilde{\mathbf{f}} \\ \mathbf{0} \end{Bmatrix}, \quad (35a)$$

and, after some manipulations, as

$$\begin{bmatrix} \frac{D_b}{L^3} \begin{bmatrix} \lambda_0^2 \tilde{\mathbf{K}}_a & \mathbf{0} \\ \mathbf{0} & \tilde{\mathbf{K}}_b \end{bmatrix} \\ b \begin{bmatrix} \tilde{\mathbf{H}}_{xx}^T & \tilde{\mathbf{H}}_{xz}^T \\ \mathbf{0} & \tilde{\mathbf{H}}_{zz}^T \end{bmatrix} \end{bmatrix} - bR_{33} \begin{bmatrix} \tilde{\mathbf{H}}_{xx} & \mathbf{0} \\ \tilde{\mathbf{H}}_{xz} & \tilde{\mathbf{H}}_{zz} \end{bmatrix} \begin{bmatrix} \begin{bmatrix} \mathbf{u}_x \\ \mathbf{q}_z \end{bmatrix} \\ \begin{bmatrix} \mathbf{r}_x \\ \mathbf{r}_z \end{bmatrix} \end{bmatrix} = \begin{bmatrix} b \begin{bmatrix} \tilde{\mathbf{f}}_a \\ \tilde{\mathbf{f}}_b \end{bmatrix} \\ \begin{bmatrix} \mathbf{0} \\ \mathbf{0} \end{bmatrix} \end{bmatrix}, \quad (35b)$$

with $\lambda_0 = L/r_g$ and the radius of gyration $r_g = h/\sqrt{12}$. Making use of Eqs. (21a,b) and (25a, b), the stiffness matrices of the i th FE read

$$\tilde{\mathbf{K}}_{a,i} = \frac{L}{l_i} \begin{bmatrix} 1 & -1 \\ -1 & 1 \end{bmatrix}, \quad (36a)$$

$$\tilde{\mathbf{K}}_{b,i} = \frac{L^3}{(1+\phi_i)l_i^3} \begin{bmatrix} 12 & -6l_i & -12 & -6l_i \\ & (4+\phi_i)l_i^2 & 6l_i & (2-\phi_i)l_i^2 \\ & & 12 & 6l_i \\ \text{symm} & & & (4+\phi_i)l_i^2 \end{bmatrix}. \quad (36b)$$

The vectors of the external load of the i th FE, Eqs, (26a, b), due to uniform load distributions $p_x(x)$, $p_z(x)$, $m(x)$ and thermal variation ΔT , are decomposed into the axial and shear-bending components as follows

$$\tilde{\mathbf{f}}_{a,i} = \frac{p_x l_i}{2} \begin{bmatrix} 1 \\ 1 \end{bmatrix} + \frac{1}{b} E_0 A_b \alpha_0 \Delta T \begin{bmatrix} -1 \\ 1 \end{bmatrix}, \quad (37a)$$

$$\tilde{\mathbf{f}}_{b,i} = p_z \begin{bmatrix} l_i/2 \\ -l_i^2/12 \\ l_i/2 \\ l_i^2/12 \end{bmatrix} + \frac{m}{(1+\phi_i)} \begin{bmatrix} 1 \\ l_i\phi_i/2 \\ -1 \\ l_i\phi_i/2 \end{bmatrix}. \quad (37b)$$

Making use of the Eqs, (27a, b, c), the elements of matrix \mathbf{H} for the generic FE have the following components

$$\tilde{\mathbf{h}}_{xx,i} = \frac{l_i}{2} \begin{bmatrix} 1 \\ 1 \end{bmatrix}, \quad \tilde{\mathbf{h}}_{zz,i} = \begin{bmatrix} l_i/2 \\ -l_i^2/12 \\ l_i/2 \\ l_i^2/12 \end{bmatrix}, \quad \tilde{\mathbf{h}}_{xz,i} = \frac{h}{2(1+\phi_i)} \begin{bmatrix} 1 \\ \phi_i l_i/2 \\ -1 \\ \phi_i l_i/2 \end{bmatrix}. \quad (38a,b,c)$$

To sum, a representation of the matrix (35b) is shown in Fig. 2, where the beam is subdivided into two elements (b_1, b_2) bonded to two substrate elements (s_1, s_2) and subjected to pointwise loads P_x, P_z, C at the beam midspan.

Owing to positive definiteness and symmetry of matrix in eq (32), system (32) can be solved through a standard algorithm. However, interesting insights may be obtained by the formal solutions of Eq. (32) that reduces to the following equations

$$\mathbf{r} = \frac{1}{R_{33}} \tilde{\mathbf{G}}^{-1} \tilde{\mathbf{H}}^T \mathbf{q}, \quad D_b/L^3 [\tilde{\mathbf{K}} + (\alpha L)^3 \tilde{\mathbf{K}}_{\text{soil}}] \mathbf{q} = b \tilde{\mathbf{f}}, \quad (39a,b)$$

being $\tilde{\mathbf{K}}_{\text{soil}} = \tilde{\mathbf{H}} \tilde{\mathbf{G}}^{-1} \tilde{\mathbf{H}}^T$ the dimensionless stiffness matrix of the substrate and

$$\alpha L = \sqrt[3]{b L^3 / (R_{33} D_b)}. \quad (40)$$

According to references [29, 30, 42, 43], the parameter αL governs the static response of the beam-substrate system. Low values of αL characterize short beams stiffer than soil, whereas high values of αL correspond to slender beams on a relatively stiff soil. Nonetheless, differently from the isotropic case, the three combinations of the elastic compliance constants (10) play a crucial role in the static response. It is worth noting that the elastic response of a thin coating bonded to an elastic substrate is characterized by the parameter $\beta L = bL/(R_{33}E_0A_b)$, yielding the relationship $(\alpha L)^3 = (\beta L) \lambda_0^2$ [29, 31, 44].

4 NUMERICAL EXAMPLES

Unless otherwise specified, a number of 512 equal beam FEs have been used. Each beam FE includes one substrate element. The solution of the system, Eq (32), provides the displacements along the centroidal beam axis and the interfacial tractions. The plotted values of horizontal interface displacement are obtained by Eq. (1a) with $z = h/2$. The axial force N , shear force V and bending moment M along the beam have been calculated through post-processing analysis, multiplying the local stiffness matrix of the beam by the displacement vector obtained by the solution of system (32).

Firstly, a Timoshenko beam loaded by a vertical force acting at the midspan is investigated in perfect adhesion or bilateral frictionless contact. Secondly, two examples of practical meaning are considered: a concrete foundation subjected to uniform vertical pressure p_z , resting on two different orthotropic soils, and a peel test of a Glass Fibre Reinforced Polymer (GFRP) wholly bonded or partially detached to a Balsa orthotropic substrate. Subsequently, a Timoshenko beam subjected to horizontal force is analysed. In particular, a shear test of GFRP reinforcement bonded to a wood substrate in perfect adhesion, with or without bending rigidity, and an aluminium reinforcement subjected to an uniform thermal variation, resting on different single wood substrate are considered. Finally, a study of a concrete foundation in perfect adhesion and in bilateral frictionless contact subjected to couple at the midspan is performed. In this case the horizontal displacement $u_{bx,0}$ of the centroidal beam axis has also been reported.

The mechanical properties used in these examples have been found in the literature, i.e. wood and plywood [45], rock [46, 47], clay [48, 49] and sand [50, 51]. Elastic modulus and Poisson's coefficients are reported in Table 1 and 2 for beams (B1, B2, B3) and substrates (S1, S2, S3, S4, S5, S6), respectively. Then, the coefficients of the substrate c_1, c_2, c_3 have been determined according to Eqs. (11) or (12).

4.1 Beam loaded by vertical force or pressure

Plane strain state is assumed for beams loaded by a vertical force P_z at the midspan or by a uniform pressure p_z and, unless specified, downward directed. Perfect adhesion and bilateral frictionless contact are considered, focusing on the behaviour of the internal shear force at the beam ends and the maximum bending moment. A GFRP reinforcement bonded to an orthotropic Balsa wood half-plane and a concrete foundation resting on an orthotropic soil are studied.

4.1.1 Beam loaded by a vertical point force P_z at the midspan

The case of GFRP Timoshenko beam, with $L/h = 10$, $\alpha L = 106.4$ and $\phi = 0.001$, perfectly bonded to an elastic orthotropic half-plane having $c_1 = 2.91$, $c_2 = 2.24$, $c_3 = 7.81$, and loaded by a vertical point force P_z acting at the midspan is reported first. The adopted elastic modulus and Poisson's coefficients of the beam B1 and substrate S1 are listed Table 1 and 2, respectively. Dimensionless displacements and reactions along the substrate boundary are shown in Figs. 3a, b, and c, d, respectively. Dimensionless values of the axial force, shear force and bending moment along the beam are shown in Figs. 3e, f and g. The cases of a beam in perfect adhesion (solid line) and in bilateral frictionless contact (dashed line) are reported.

The horizontal displacement u_x corresponding to the frictionless condition produces a contraction of the half-plane surface along the whole interface. Conversely, a different behaviour occurs in the case of a beam in perfect adhesion, owing to the fact that u_x is affected by the contribution of the term $\phi h/2$ also. Indeed, in such a condition, Fig. 3a shows a non-monotonic trend for the horizontal displacement which changes its sign into a narrow central region (i.e. $-0.1 < x/L < 0.1$). At the beam ends, the horizontal displacement assumes a value 10 times lower than those found for the bilateral frictionless contact. The maximum value of the vertical displacement u_z is achieved at the midpoint ($x/L = 0$) and, in perfect adhesion, it results 20% lower than that found for a beam in perfect contact with the half-plane, as shown in Fig. 3b. For a beam in perfect adhesion, the tangential reaction r_x at $x/L = 0$ and at the beam ends exhibits a finite discontinuity, whereas it is equal to zero for a beam in bilateral frictionless contact, as reported in Fig. 3c. As expected, a singular normal reaction r_z at the midspan is found, as shown in Fig. 3d. Note also that the peel tractions at the beam ends assume different sign depending upon the contact condition. This aspect was already remarked in [29, 30]. The axial force of the beam in perfect adhesion is shown in Fig. 3e. Shear force and bending moment are not significantly affected by the contact condition, as displayed in Figs. 3f and g.

An accurate description of the shear force is obtained using the beam T1 with $L/h = 40$, see Fig. 4. The comparison is made among an Euler-Bernoulli ($\phi = 0$) and two Timoshenko beams ($\phi = 10^{-2}$ and 10^{-5}) in perfect adhesion (solid line) and in bilateral frictionless contact (dashed line) versus the dimensionless coordinate x/L . The orthotropic substrate S1 is considered, leading to $\alpha L = 42.5$. Fig. 4a shows that the shear force of a Timoshenko beam with small value of ϕ is analogous to that of an Euler-Bernoulli beam, except at the beam ends. The response in terms of shear force is analyzed in detail at the beam ends, using a logarithmically spaced mesh in the interval $[0.4, 0.5 - 10^{-4}]$, where different behaviour between Euler-Bernoulli and Timoshenko beams is found. In particular, a singularity of the shear force for the Euler-Bernoulli beam is observed (see Fig. 4b). Conversely, for beams in bilateral frictionless contact with the half-plane, the shear force does not depend significantly on the kind of beam adopted, and it assumes vanishing values at the beam ends.

The maximum bending moment of concrete beams resting on an elastic medium is a key issue in the framework of civil engineering, with particular reference to the design of shallow foundation of buildings. Euler-Bernoulli ($\phi = 0.0$) and Timoshenko ($\phi = 0.03$) concrete foundation beams, loaded by a vertical point force P_z at the midspan and resting on an isotropic or orthotropic soil, are considered. Dimensionless maximum bending moment at $x/L = 0$ versus αL is reported for a beam in bilateral frictionless contact (Figs. 5a, b) and in perfect adhesion (Figs. 5 c, d), respectively. The elastic parameters $c_1 = 0.84$, $c_2 = 2.15$, $c_3 = 0.62$, and $E_3 = 0.12$ MPa are taken for the orthotropic soil (solid line), while the same Young's modulus is assumed (dash-dot line) for the isotropic soil. Table 1 and 2 show the elastic moduli and Poisson's coefficients of the adopted beam T2 and soil S2.

In bilateral frictionless contact, the maximum bending moment, M_{\max} , of a flat rigid indenter loaded by a vertical force P_z , may be calculated by integrating from 0 to $L/2$ the moment induced by the pressure r_z given by Sadowsky [4, 6] with respect to the midspan, namely

$$M_{\max} = \int_0^{L/2} r_z x dx = \frac{P_z L}{2\pi} \cong 0.1592 P_z L, \quad (41)$$

where the pressure is given by

$$r_z(x) = \frac{P_z}{\pi\sqrt{(L/2)^2 - x^2}}. \quad (42)$$

As shown in Fig. 5a, the maximum value of the bending moment for $\alpha L \leq 1$ agrees well with that predicted by the Sadowsky solution. The magnitude of maximum bending moment decreases as αL increases, hence for flexible or long beams. According to Biot [42], the maximum bending moment of an infinite Euler-Bernoulli beam resting on isotropic substrate in bilateral frictionless contact reads

$$M_{\max} = \frac{P_z a}{\pi} \int_0^\infty \frac{a}{a^3 + 1} da = \frac{2}{3\sqrt{3}} P_z a \cong 0.4849 \frac{P_z L}{\alpha L}, \quad (43)$$

where $a = \sqrt[3]{2} L / \alpha L$.

It is worth noting from Fig. 5b that the maximum bending moment provided by Eq. (43) holds for $\alpha L > 10$. Conversely, for an infinite Timoshenko beam is not possible to obtain a constant value. Note also that, for $\alpha L > 5$, the maximum bending moment obtained by considering the orthotropic half-plane results about 5% lower than that found for an isotropic half-plane.

For the perfect adhesion condition, the maximum bending moment of a rigid flat punch loaded by a vertical force P_z , acting on an elastic isotropic substrate, could be obtained by integrating the normal and shear tractions given by Abramov [6]:

$$r_z(x) = \frac{1 + \kappa}{\sqrt{\kappa}} \frac{P_z}{2\pi\sqrt{(L/2)^2 - x^2}} \cos\left(\frac{\ln \kappa}{2\pi} \ln \frac{L/2 + x}{L/2 - x}\right), \quad (44a)$$

$$r_x(x) = \frac{1 + \kappa}{\sqrt{\kappa}} \frac{P_z}{2\pi\sqrt{(L/2)^2 - x^2}} \sin\left(\frac{\ln \kappa}{2\pi} \ln \frac{L/2 + x}{L/2 - x}\right), \quad (44b)$$

within the contact region $0 \leq x < L/2$ multiplied by their distance from the centroid of the rigid punch, as follows

$$M_{\max} = \int_0^{L/2} (r_z x - r_x h/2) dx \cong (0.1522 - 0.0795 h/L) P_z L \cong 0.1443 P_z L, \quad (45)$$

by assuming $L/h = 10$, $\kappa = 2.44$, that is $\kappa = (3 - \nu_s)/(1 + \nu_s)$ or $\kappa = 3 - 4\nu_s$ for a generalized plane stress or plane strain state, with the Poisson coefficient of isotropic substrate ν_s equal to 0.16 or 0.14 respectively. As shown in Fig. 5c, Eq. (45) holds for both beams (Euler-Bernoulli and Timoshenko) bonded to an elastic isotropic or orthotropic substrate with $\alpha L \leq 1$. Finally, the maximum bending moment of a beam bonded to a substrate in perfect adhesion is 10% lower than that found for a beam in bilateral frictionless contact because of the presence of tangential tractions r_x . The analytic solution of M_{\max} of an infinite beam resting on a substrate in perfect adhesion is not present in the literature. However, the numerical solutions displayed in Fig. 5d show a decrease in the maximum value of the bending moment, whereas for a beam in perfect adhesion, for $\alpha L = 10$ it is approximately 20% less than that found for the bilateral frictionless contact condition for both the beam theories. For a beam in the perfect adhesion with the half-plane, the M_{\max} obtained by considering the orthotropic half-plane results about 10% lower than that obtained for an isotropic substrate for $\alpha L > 5$.

4.1.2 Comparison with standard FE model

In order to assess the numerical performance of the present model as compared with conventional FEs, a beam perfectly bonded to an elastic half-plane is analysed by means of standard FE model. Quadrilateral FEs in plane state are used to simulate the substrate, which displacements in the normal direction of the boundaries are restrained. As shown in Fig. 6, three different square

substrate meshes with total width equal to $8L$ (FEM 8L), $16L$ (FEM 16L) and $32L$ (FEM 32L) are analysed (this latter is not shown in Fig. 6 because its large dimensions), being L the beam span length. FEM 16L and FEM 32L meshes are introduced to provide a more accurate description of the beam horizontal displacement, which is expected to be significant for most of the beam length, particularly for slender beams. Two refined square meshes, having widths equal to $4L$ and $2L$ for FEM 8L, to $8L$ and $4L$ for FEM 16L, and to $16L$ and $8L$ for FEM 32L, are carried out near the foundation beam. The case of the foundation beam subdivided into 4 beam FEs for meshes FEM 8L and FEM 16L is displayed in Figs. 6a, 6b, respectively. A precise solution of the soil-structure interaction problem can be obtained by using the adopted meshes which involve a number of FEs lower than that required by a uniform mesh of quadrilateral elements.

Indicating with n_{el} the number of beam FEs, the number of equations associated with meshes FEM 8L, FEM 16L and FEM 32L is given by $n_{eq}^{(8L)} = 20.1 n_{el}^2$, $n_{eq}^{(16L)} = 80.4 n_{el}^2$ and $n_{eq}^{(32L)} = 321.6 n_{el}^2$, respectively (note that, for meshes FEM 8L and FEM 16L, the case for $n_{el} = 4$ is depicted in Figs. 6a, 6b), whereas the number of equations, n_{eq} , associated with the Present Analysis (PA) is given by $n_{eq}^{(PA)} = 5 n_{el} + 3$. In order to compare the two formulations, reference is made to the GFRP Timoshenko beam previously investigated. For each of the numerical models compared, a series of mesh refinements is obtained by letting n_{el} progressively takes the values 8, 16, 32, 64, 128, 254, 512 and 1024. Comparison is made by taking as a base solution the numerical solution obtained through the PA by discretizing the beam with 4096 equal FEs.

Fig. 7 shows the test results in terms of relative error $e_M = |M_{\max} - M_{\text{ref}}| / |M_{\text{ref}}|$ versus the number of equations n_{eq} , where M_{\max} represents the peak value of the bending moment in the beam obtained from the various models for a generic discretization, and M_{ref} denotes the maximum bending moment corresponding to the reference solution. In particular, $M_{\text{ref}} = +0.005796 P_z L$ (sagging bending moment with tension in bottom fibres).

As shown in Fig. 7 and Table 3, the proposed model gives more accurate results and it exhibits higher convergence rate with respect to conventional FE model. In particular, for a fixed number of equations n_{eq} , Fig. 7 shows that the present approach provides peak values of the maximum bending moment of the beam affected by relative errors that are much lower than those obtained by using a standard FE formulation. Furthermore, the proposed model is characterized by a high rate of convergence $C n_{eq}^{-\lambda}$ as it yields an exponent λ significantly larger than those provided by standard FE model, as shown in Table 3 for the curves displayed in Fig. 7.

Such results confirm that the present model is a valid tool to solve properly beam-substrate interaction problems by using a small number of beam FEs. In particular, it is shown a number $n_{el} = 512$ of equal beam FEs gives accurate solutions for all cases considered afterwards.

4.1.3 Foundation loaded by a vertical pressure p_z over length $L/4$ at the midspan

In this Section, the case of a Timoshenko beam subjected to a uniform vertical load distribution p_z acting over a length $L/4$ centered with respect to the midspan is analysed. Dimensionless interface displacements, soil reactions, axial force, shear force, and bending moment along the beam, are reported in Fig. 8.

Two kinds of orthotropic soil in perfect adhesion with the beam are studied. Assuming the elastic modulus and Poisson's coefficient of concrete beam T2 listed in Tab.1, clay S2 or sand soil S3 in Tab. 2 the soil coefficients are $c_1 = 0.84$, $c_2 = 2.15$, $c_3 = 0.62$ for clay soil or $c_1 = 1.06$, $c_2 = 2.15$, $c_3 = 0.93$ for sand soil. Assuming a ratio $L/h = 10$ for the beam, the parameter αL becomes equals 3.65 or 4.54, respectively.

Displacements u_x and u_z at the substrate boundary for perfect adhesion condition are reported in Fig. 8a and b respectively, for both soils. It is worth noting that for a beam resting on a relatively rigid soil (i.e. $\alpha L = 4.54$, dashed line), the horizontal interface displacement at the beam end and the vertical interface displacement at $x/L = 0$ are 30% and 60% higher, respectively, than those

calculated for a beam bonded to a relatively soft soil (i.e. $\alpha L = 3.65$, solid line), whereas both substrate reactions are quite similar, as shown in Fig. 8c and 8d. Conversely, the axial force of the beam resting on a relatively rigid soil (Fig. 8e, dashed line) is about 15% lower than that obtained by considering a soft soil. However, almost the same values of the shear force and bending moment along the beam are found for both the orthotropic soils. The shear force obtained by considering the Euler-Bernoulli beam ($\phi = 0.0$) with $\alpha L = 3.65$ in perfect adhesion with the soil is also displayed in Fig. 8f (thin solid line). It is worth noting that going toward the beam ends, a completely different behaviour of the shear force is observed with respect to that found for the Timoshenko beam. In particular, the shear force for an Euler-Bernoulli beam takes non zero values and opposite sign with respect to those obtained by considering a Timoshenko beam.

4.1.4 Detached beam loaded by a vertical point force P_z at one end

A GFRP stiffener subjected to a vertical point force P_z applied at one end and upward directed, bonded to a Balsa orthotropic substrate in perfect adhesion, is investigated here. Elastic moduli and Poisson's coefficients are reported in Tab. 1 and 2, respectively, for the beam T1 and the substrate S1.

Dimensionless interfacial displacements and substrate reactions are shown in Figs. 9a-d, whereas the axial force, shear force and bending moment are displayed in Figs. 9e-g, for a beam detached from the substrate between $x/L = 0.3$ and $x/L = 0.40$ (solid line) and a fully bonded beam (dashed line). In particular, for the detached beam, a number of 297 logarithmically spaced FEs are used, and the length of the beam has been subdivided in four intervals to capture straightforwardly the stress singularity. Thus a number of 84 logarithmically spaced points are generated in the interval $[-0.5+10^{-8}, -0.1]/L$, 85 points in the intervals $[-0.1, 0.3]/L$, 65 points into $[0.4, 0.45]/L$, and 64 points into $[0.45, 0.5-10^{-8}]/L$. The results concerned with the detached beam are almost identical to those obtained for the fully bonded beam, except in the neighbourhood of the detached region. In particular, at the ends of the detached region both the shear and peel stresses appear to be singular.

Moreover, as expected, zero substrate reaction and constant axial force are found within the detached region.

4.2 Beam loaded by horizontal force or subjected to uniform thermal load ΔT

Plane stress state is assumed for a beam bonded to an orthotropic substrate and loaded by horizontal force P_x or subjected to uniform thermal load ΔT . Two examples of practical relevance are considered: a GFRP or aluminium stiffener bonded to an orthotropic wood substrate. Moreover, the shear force of Euler-Bernoulli and Timoshenko beams are compared along the contact length and at one end.

4.2.1 GFRP beam loaded by a horizontal point force P_x at one end

The case of an elastic Timoshenko beam T1 loaded by a horizontal concentrated force acting at one end, perfectly bonded to a wood orthotropic substrate S4, is analysed and compared with a beam having a vanishing bending rigidity (thin film assumption) in Fig. 10. Assuming $L/h = 60$, the governing parameter for the beam is $\alpha L = 40.2$ (solid line), whereas $\beta L = 1.50$ (dashed line) holds for the membrane assumption.

Dimensionless interface displacements or substrate reactions for both cases are similar, except the normal component of the interfacial stress field, which is zero within the whole contact region for the case of a thin film. It is worth noting that the normal component of the displacement quickly grows going toward the ends of the stiffener, particularly for the case of the Timoshenko beam. Note also that the peel stress changes its sign in the neighbourhoods of the beam ends, similarly to the case of a beam loaded by a vertical pointwise force acting at the midspan (see Fig. 3d). Moreover, a peak value for the peel stress occurs in the neighbouring of the load section, as shown in Fig. 8d. Besides, the shear force and the bending moment could be found for the beam case only. However, the solution of the beam-substrate interaction problem where only horizontal forces act on the system does not appreciably depend on the parameter ϕ [29]. Hence, concerning this loading

condition, the choice of Euler-Bernoulli or Timoshenko beam model leads to almost the same results.

Conversely, the shear force is significantly affected by the shear deformation of the beam. This fact has been found by investigating a Timoshenko beam loaded by a horizontal pointwise force acting at one end of the beam varying the parameter ϕ . In particular, an Euler-Bernoulli beam ($\phi = 0$) and a Timoshenko beam with $\phi = 10^{-2}$ and 10^{-5} have been studied in detail. Fig. 11 shows the shear force along the beam and in the neighbourhood of the external force. As expected, the shear force of a Timoshenko beam with small ϕ tends to that of an Euler-Bernoulli beam. However, the main differences occur in the neighbourhood of the loaded section, where the shear force of the Euler-Bernoulli beam takes opposite sign and does not vanish at the beam ends. Conversely, the shear force of a Timoshenko beam at the loaded section vanishes, and going toward the inner part of the contact region, it increases in magnitude as the parameter ϕ increases. Note also that the maximum value achieved by the shear force of a Timoshenko beam occurs at about $0.47 \div 0.48 x/L$, whereas in an Euler-Bernoulli beam it occurs in the range $0.46 \div 0.47 x/L$.

4.2.2 Stiffener subjected to uniform thermal load ΔT

The behaviour of a beam resting on an elastic substrate and subjected to a uniform thermal variation ΔT resembles that of a beam symmetrically loaded by two opposite axial forces applied at the beam ends, as shown for the bar-substrate problem [31]. The interaction between an aluminium stiffener and a wood substrate is investigated. The Euler-Bernoulli beam theory is assumed and two kinds of orthotropic half-plane are studied, as shown in Fig. 12. The elastic moduli and Poisson's coefficients of the beam T3 and the substrates S5 or S6 are listed in Table 1 and 2, respectively. In particular, two kinds of half-plane having the same Young modulus in z -direction and characterised by $c_1 = 0.45$, $c_2 = 1.95$, $c_3 = 0.20$ (S5, solid line), and $c_1 = 0.65$, $c_2 = 2.90$, $c_3 = 0.40$ (S6, dashed line) are

considered. Therefore, by taking a length-to-height ratio $L/h = 10$, both cases are characterized by the parameter $\alpha L = 60$.

Dimensionless interface displacements and substrate reactions versus x/L are plotted in Fig. 12a, b and c, d, respectively. The axial force, shear force and bending moment of the beam are shown in Fig. 12e, f and g. It is worth remarking that the substrate S5 having a high elastic stiffness in x -direction (solid line) exhibits a horizontal component of the interfacial displacement 25% lower than that found for the compliant substrate S6 (dashed line). Conversely, the vertical component of the interfacial displacement is 60% higher with respect that exhibited by the wood substrate S6. On the other hand, shear and normal components of the interfacial stress field for a substrate having a low value of Young modulus in x -direction (namely, the substrate S6), are quite uniform along the beam, with relatively low peak values attained at the beam ends, see Fig. 12c, 12d. This circumstance holds for the axial force, shear force and bending moment also, which magnitude decrease by assuming the wood substrate S6. Note also that the peel tractions change sign in the range $0.3 \div 0.4 x/L$ for both the substrates. For comparison, in Fig. 12f the shear force of a Timoshenko beam ($\phi = 0.03$) is also reported, which vanishes at the end sections, as expected. Similarly to the previous loading condition, also for the case of a uniform thermal variation, the shear force of an Euler-Bernoulli beam in the neighbourhoods of the beam ends changes its sign with respect that found for a Timoshenko beam.

4.3 Beam loaded by a couple

A concrete foundation loaded by a counter-clockwise couple C acting at the midspan and resting on an orthotropic soil is investigated in this Section. Fig. 13 shows the results of a Timoshenko beam T2 with $L/h = 10$ and $\phi = 0.03$ in perfect adhesion (solid line) and in bilateral frictionless contact (dashed line) with an orthotropic soil S2 having $c_1 = 0.84$, $c_2 = 2.15$, $c_3 = 0.62$.

The horizontal component of the interfacial displacement of a Timoshenko beam perfectly welded to the half-plane assumes an opposite sign and values lower (in modulus) than those found

for a beam in bilateral frictionless contact, as displayed in Fig. 13a. In the same figure is also plotted the displacement at the centreline $u_{bx,0}$ of a beam perfectly bonded to the substrate, thus confirming the relevance of the term $\varphi h/2$ affecting the horizontal component of the displacement field. The vertical component of the interfacial displacement of a beam in perfect adhesion is almost the same of that of a beam in bilateral frictionless contact, as shown in Fig. 13b. The same circumstance holds for the peel tractions except at the loaded section, where the peel tractions of a Timoshenko beam in perfect adhesion with the half-plane exhibit a discontinuity. As expected, the shear reaction and, in turn, the normal force along the beam are zero when bilateral frictionless contact is supposed. It is worth noting that the shear tractions of a Timoshenko beam in perfect adhesion with the half-plane are singular across the loaded section. The axial force, shear force and bending moment of the beam are shown in Fig. 13e, 13f and 13g, respectively. Note that the axial force attains the maximum value at about $0.3 x/L$ and, owing to symmetry, it vanishes at $x = 0$. Moreover, the shear force and bending moment are not significantly affected by the contact condition. For both the contact conditions here considered, the maximum value achieved by the shear force turns out to be $1.5 C/L$ and it occurs at $x = 0$. Moreover, $|M(0^+)| = |M(0^-)| = C/2$, as expected due to symmetry.

CONCLUSIONS

A coupled FE-BIE method for the analysis of a prismatic beam bonded to an elastic orthotropic half-plane is considered in plane stress and plane strain state. The mixed variational formulation is obtained through the theorem of work and energy for exterior domain. Unknown functions are represented by beam displacements and surface tractions by means of classical FE method and BIE approach, respectively. A generalised Green function of orthotropic half-plane, characterised by three substrate coefficients, has been used, thus providing the relationship between displacements and interface reactions. Linear shape function is selected to approximate axial displacement, whereas cubic and quadratic shape functions are used to interpolate transverse deflection and

rotation, respectively. Shear and normal surface tractions are described by piecewise constant shape functions.

The proposed method is utilised to study in detail the contact problem of a finite elastic Timoshenko beam bonded to an orthotropic half-plane in perfect adhesion as well as in bilateral frictionless contact. The case of a beam having a vanishing bending rigidity has been investigated also. In particular, when shear tractions and external horizontal forces are set to zero, the proposed formulation resembles a bilateral frictionless contact. The thin film problem can be properly handled by neglecting the beam bending rigidity. Moreover, through post-processing analysis, the axial force, shear force and bending moment of the beam are determined. The use of the Timoshenko beam theory to analyse the effects induced by the shear deformation leads to values for the internal shear force sensibly different than that calculated by assuming the Euler-Bernoulli theory.

A variety of examples of practical relevance are presented and discussed considering a beam loaded by a horizontal or vertical force and a couple. In the case of a beam subjected to a vertical point force it is shown that the relative stiffness of beam-substrate significantly affects the maximum bending moment. Moreover, for such a loading condition, the peel tractions display a singular behaviour just across the loaded section for both the contact conditions considered in the analysis. The analytic solutions available in the literature for the problem of the rigid punch and the maximum bending moment of an infinite Euler-Bernoulli beam resting on an isotropic substrate are retrieved. Furthermore, the present model can be used in forthcoming studies in the framework of contact mechanics. As an example, peel or shear tests of GFRP or aluminium stiffeners bonded to wood substrate are analysed. The case of a detached or fully bonded beam has been investigated also, finding almost the same results, except in the region close to the detachment. Furthermore, a stiffener subjected to a uniform thermal variation has been studied, showing a decrease in the stress response for orthotropic substrates having the same elastic modulus in z -direction and lower in x -direction. Finally, in the last application regarding the soil-foundation interaction when a

concentrated couple acts at the beam midspan, the contact condition (i.e., perfect adhesion or bilateral frictionless contact) does not significantly affect the response of the system, except for the horizontal displacement. It must be remarked that, for a beam perfectly welded to the substrate subjected to a such a loading condition, the shear tractions appear to be singular whereas the peel stress displays a finite jump across the loaded section.

ACKNOWLEDGMENTS

The present investigation was developed in the framework of the Research Program FAR 2014 of the University of Ferrara. Moreover, the analyses were developed within the activities of the (Italian) University Network of Seismic Engineering Laboratories–ReLUIS in the research program funded by the (Italian) National Civil Protection – Progetto Esecutivo 2014-2016 – Research Line “Reinforced Concrete Structures” and “Innovative materials”. Finally, L.L. gratefully acknowledges financial support from National Group of Mathematical Physics GNFM-INdAM (Progetto Giovani 2015).

REFERENCES

- [1] Teng JG, Chen JF, Smith ST, Lam L. FRP strengthened RC structures. Chichester: John Wiley & Sons; 2001.
- [2] Zhao X-L. FRP-strengthened metallic structures. Boca Raton: CRC Press; 2014.
- [3] Schobera K-U, Harteb AM, Kligerc R, Jockwerd R, Xue Q, Chenf J-F. FRP reinforcement of timber structures. *Constr Build Mater* 2015; 97:106–118.
- [4] Galin LA. Contact Problems. The legacy of L.A. Galin. Netherlands: Springer; 2008.
- [5] Johnson KL. Contact mechanics. Cambridge: Cambridge University Press; 1985.
- [6] Kachanov ML, Shafiro B, Tsukrov I. Handbook of elasticity solutions. Dordrecht: Kluwer Academic Publishers; 2003.
- [7] Lekhnitskii SG. Theory of elasticity of an anisotropic body. Moscow: MIR Publishers; 1977.
- [8] Gladwell GML. Contact problems in the classical theory of elasticity. The Netherlands: Sijthoff & Noordhoff; 1980.
- [9] Willis JR. The elastic interaction energy of dislocation loops in anisotropic media. *Q J Mech Appl Math* 1965; 18(4):419–433.
- [10] Pan YC, Chou TW. Point force solution for an infinite transversely isotropic solid. *J Appl Mech ASME* 1976; 43(4):608–612.
- [11] Pan YC, Chou TW. Green's functions for two-phase transversely isotropic materials. *J Appl Mech ASME* 1979; 46(3):551–556.
- [12] Wu RS, Chou YT. Line force in a two-phase orthotropic medium. *J Appl Mech ASME* 1982; 49:55–61.
- [13] Lin W, Kuo CH, Keer LM. Analysis of a transversely isotropic half-space under normal and tangential loadings, *J Tribol ASME* 1991; 113(4):335–338.
- [14] Lanzoni L, Radi E. Thermally induced deformations in a partially coated elastic layer. *Int J Solids Struct* 2009; 46(6):1402–1412.

- [15] Lanzoni L. Analysis of stress singularities in thin coatings bonded to a semi-infinite elastic substrate. *Int J Solids Struct* 2011; 48(13):1915–1926.
- [16] Lanzoni L, Radi E. A loaded Timoshenko beam bonded to an elastic half plane. *Int J Solids Struct* 2016; 92–93:76–90.
- [17] Gallagher AP. Bending of a free beam on an elastic foundation. *J Appl Mech ASME* 1983; 50(2):463–465.
- [18] Shield TW, Kim KS. Beam theory models for thin film segments cohesively bonded to an elastic half space. *Int J Solids Struct* 1992; 29(9):1085–1103.
- [19] Li H, Dempsey JP. Unbonded contact of finite Timoshenko beam on elastic layer. *J Eng Mech* 1988; 114(8): 1265–1284.
- [20] Zhang Y-M, Gu Y, Chen J-T. Internal stress analysis for single and multilayered coating systems using the boundary element method. *Eng Anal Bound Elem* 2011; 35(4):708–717.
- [21] Freund LB, Suresh S. *Thin film materials. Stress, defect formation and surface evolution.* Cambridge: Cambridge University Press; 2008.
- [22] Bush MB. Simulation of contact-induced fracture. *Eng Anal Bound Elem* 1999; 23(1):59–66.
- [23] Rudas M, Bush MB, Reimanis IE. The kinking behaviour of a bimaterial interface crack under indentation loading. *Eng Anal Bound Elem* 2004; 28(12): 1455–1462.
- [24] Ribeiro DB, Paiva JB. An alternative BE–FE formulation for a raft resting on a finite soil layer. *Eng Anal Bound Elem* 2015; 50:352–359.
- [25] Luo JF, Liu YJ, Berger EJ. Analysis of two-dimensional thin structures (from micro-to nano-scales) using the boundary element method, *Comput Mech* 1998; 22(5):404–412.
- [26] Gu Y, Chen W, Zhang B. Stress analysis for two-dimensional thin structural problems using the meshless singular boundary method. *Eng Anal Bound Elem* 2015; 59:1–7.
- [27] Cheung YK, Zienkiewicz OC. Plates and tanks on elastic foundations - an application of finite element method. *Int J Solids Structure* 1965; 1(4):451–461.

- [28] Cheung YK, Nag DK. Plates and beams on elastic foundation - linear and non-linear behaviour. *Geotechnique* 1968; 18(2):250–260.
- [29] Tezzon E, Tullini N, Minghini M. Static analysis of shear flexible beams and frames in adhesive contact with an isotropic elastic half-plane using a coupled FE-BIE model. *Eng Struct* 2015; 104:32–50.
- [30] Tullini N, Tralli A. Static analysis of Timoshenko beam resting on elastic half-plane based on the coupling of locking-free finite elements and boundary integral. *Comput Mech* 2010; 45(2–3):211–225.
- [31] Tullini N, Tralli A, Lanzoni L. Interfacial shear stress analysis of bar and thin film bonded to 2D elastic substrate using a coupled FE-BIE method. *Finite Elem Anal Des* 2012; 55:42–51.
- [32] Tullini N, Tralli A, Baraldi D. Stability of slender beams and frames resting on 2D elastic half-space. *Arch Appl Mech* 2013; 83(3):467–482.
- [33] Tullini N, Tralli A, Baraldi D. Buckling of Timoshenko beams in frictionless contact with an elastic half-plane. *J Eng Mech* 2013; 139(7):824–831.
- [34] Reinoso J, Paggi M, Rolfes R. A computational framework for the interplay between delamination and wrinkling in functionally graded thermal barrier coatings, *Comput Mater Sci* 2016; 116, 82–95.
- [35] Cowper GR. The shear coefficient in Timoshenko's beam theory. *J Appl Mech ASME* 1966; 33:335–340.
- [36] Tullini N, Savoia M. Elasticity interior solution for orthotropic strips and the accuracy of beam theories. *J Appl Mech ASME* 1999; 66(2):368–373.
- [37] Gurtin ME, Sternberg E. Theorems in linear elastostatics for exterior domains. *Arch Ration Mech Anal* 1961; 8:99–119.
- [38] Narayanaswami R, Adelman HM. Inclusion of transverse shear deformation in finite element displacement formulations. *AIAA J* 1974; 12(11):1613–1614.

- [39] Friedman Z, Kosmatka JB. An improved two-node Timoshenko beam finite element. *Comput Struct* 1993; 47(3):473–481.
- [40] Reddy JN. On locking-free shear deformable beam finite elements. *Comput Meth Appl Mech Eng* 1997; 149(1-4):113–132.
- [41] Minghini F, Tullini N, Laudiero F. Locking-free finite elements for shear deformable orthotropic thin-walled beams. *Int J Numer Methods Eng* 2007; 72(7):808–834.
- [42] Biot MA. Bending of an infinite beam on an elastic foundation. *J Appl Mech* 1937; 4:A1–A7.
- [43] Vesic AB. Bending of beams on isotropic elastic medium. *J Eng Mech Div ASCE* 1961; 87(EM2):35–53.
- [44] Grigolyuk EI, Tolkachev VM. Contact problems in the theory of plates and shells, Moscow: Mir Publishers; 1987.
- [45] Forest Products Laboratory. Wood handbook. Wood as an engineering material. General Technical Report FPL-GTR-190. Madison, WI: U.S. Department of Agriculture, Forest Service, Forest Products Laboratory; 2010.
- [46] Kolar V, Nemeč I. Modelling of soil-structure interaction. *Developments in geotechnical engineering* 58. Amsterdam: Elsevier; 1989.
- [47] Thomsen L. Weak elastic anisotropy. *Geophysics* 1986; 51(10):1954–1966.
- [48] Yimsiri S, Soga K. Cross-anisotropic elastic parameters of two natural stiff clays. *Geotechnique* 2011; 61(9):809–814.
- [49] Ratananikom W, Likitlersuang S, Yimsiri S. An investigation of anisotropic elastic parameters of Bangkok Clay from vertical and horizontal cut specimens. *Geomech Geoeng* 2013; 8(1):15–27.
- [50] Bellotti R, Jamiolkowski M, Lo Presti DCF, O'Neill DA. Anisotropy of small strain stiffness in Ticino sand. *Geotechnique* 1996; 46(1):115–131.
- [51] Schadlich B, Schweiger HF. Influence of anisotropic small strain stiffness on the deformation behavior of geotechnical structures. *Int J Geomech* 2013; 13:861–868.

Figure Captions

Fig. 1. Beam under general loads bonded to an orthotropic half-plane.

Fig. 2. Matrix system of a beam subdivided in two beam elements b_1, b_2 , each of which is bonded to a single substrate element s_1, s_2 , respectively. External pointwise loads P_x, P_z and couple C applied at the middle.

Fig. 3. GFRP Timoshenko beam ($L/h = 100, \alpha L = 106.4$ and $\phi = 0.001$) loaded by a vertical force P_z at the midpoint and bonded to a Balsa orthotropic half-plane in plane strain state ($c_1 = 2.91; c_2 = 2.24; c_3 = 7.81$) in perfect adhesion (solid line) and in bilateral frictionless contact (dashed line). Dimensionless values of u_x (**a**), u_z (**b**), r_x (**c**), r_z (**d**), N (**e**), V (**f**), M (**g**) versus x/L .

Fig. 4. GFRP Euler-Bernoulli ($\phi = 0$) and Timoshenko beams ($\phi = 10^{-2}$ and 10^{-5}) with $L/h = 40$ loaded by a vertical force P_z at the midpoint and bonded to Balsa orthotropic half-plane in plane strain state ($c_1 = 2.91; c_2 = 2.24; c_3 = 7.81$) in perfect adhesion $\alpha L = 42.5$ (solid line) and in bilateral frictionless contact for GFRP Euler-Bernoulli beam ($\phi = 0$) (dashed line). Shear force V along the beam (**a**) and at the beam end (**b**).

Fig. 5. Concrete beam loaded by a vertical force P_z at the midpoint, bonded to an orthotropic soil with $c_1 = 0.84; c_2 = 2.15; c_3 = 0.62; E_3 = 0.12\text{MPa}$ (solid line) and isotropic soil (dash-dot line). Bending moment M at the midspan versus αL of a beam in bilateral frictionless contact (**a, b**) and in perfect adhesion (**c, d**) for $\phi = 0.0$ and $\phi = 0.03$ (thin and thick line, respectively).

Fig. 6. Meshes adopted for the two-dimensional FE models with a beam subdivided into 4 equal FEs. Models with mesh dimension $8L$ (FEM 8L) (**a**) and $16L$ (FEM 16L) (**b**).

Fig. 7. GFRP Timoshenko beam ($L/h = 100, \alpha L = 106.4, \phi = 0.001$) loaded by a vertical force P_z at the midpoint and bonded to a Balsa orthotropic half-plane in plane strain ($c_1 = 2.91; c_2 = 2.24; c_3 = 7.81$). Relative errors of maximum bending moment $e_M = |M_{\max} - M_{\text{ref}}| / |M_{\text{ref}}|$ versus number of equations n_{eq} for the present analysis (PA) and for meshes FEM 8L, FEM 16L and FEM 32L.

Fig. 8. Concrete beam subjected to an uniform vertical load distribution p_z acting over a length $L/4$ centered with respect to the midspan, resting on an orthotropic soil. Timoshenko beam ($L/h = 10$, $\phi = 0.03$) bonded to two kinds of orthotropic half-planes in perfect adhesion, $c_1 = 0.84$; $c_2 = 2.15$; $c_3 = 0.62$; $\alpha L = 3.65$ (solid line) and $c_1 = 1.06$; $c_2 = 2.15$; $c_3 = 0.93$; $\alpha L = 4.54$ (dashed line). Shear force V of an Euler-Bernoulli beam bonded to a half-plane with $c_1 = 0.84$; $c_2 = 2.15$; $c_3 = 0.62$; $\alpha L = 3.65$ (thin solid line in **f**).

Fig. 9. GFRP Timoshenko beam ($L/h = 20$, $\alpha L = 21.3$ and $\phi = 0.02$) loaded by a vertical force P_z acting at a beam end and detached between $x/L=0.3$ and $x/L = 0.4$ (solid line) and perfectly bonded (dashed line) to Balsa orthotropic half-plane in plane strain state ($c_1 = 2.91$; $c_2 = 2.24$; $c_3 = 7.81$). Dimensionless values of u_x (**a**), u_z (**b**), r_x (**c**), r_z (**d**), N (**e**), V (**f**), M (**g**) versus x/L .

Fig. 10. GFRP Timoshenko beam ($L/h = 60$ and $\phi = 0.003$ with $c_1 = 0.70$; $c_2 = 2.40$; $c_3 = 0.44$) loaded by a horizontal force P_x acting at one end and bonded to a wood orthotropic half-plane in plane stress state ($c_1 = 0.56$; $c_2 = 2.22$; $c_3 = 0.28$) with $\alpha L = 40.2$ (solid line), and thin film assumption with $\beta L = 1.50$ (dashed line). Dimensionless values of u_x (**a**), u_z (**b**), r_x (**c**), r_z (**d**), N (**e**), V (**f**), M (**g**) versus x/L .

Fig. 11. GFRP Euler-Bernoulli ($\phi = 0$) and Timoshenko beams ($\phi = 10^{-2}$ and 10^{-5}) with $L/h = 60$ loaded by a horizontal force P_x acting at one end and bonded to a wood orthotropic half-plane in plane stress state ($c_1 = 0.56$; $c_2 = 2.22$; $c_3 = 0.28$) with $\alpha L = 40.2$. Shear force V along the beam (**a**) and at the beam end (**b**).

Fig. 12. Aluminium stiffener subjected to an uniform thermal variation $+\Delta T$ bonded to a wooden substrate. Euler-Bernoulli beam ($L/h = 10$, $\alpha L = 60$) resting on two kinds of orthotropic half-plane with $c_1 = 0.45$; $c_2 = 1.95$; $c_3 = 0.20$ (solid line) and $c_1 = 0.65$; $c_2 = 2.90$; $c_3 = 0.40$ (dashed line) in perfect adhesion. Dimensionless values of u_x (**a**), u_z (**b**), r_x (**c**), r_z (**d**), N (**e**), V (**f**), M (**g**) versus x/L . Shear force V of a Timoshenko beam ($\phi = 0.03$) bonded to half-plane with $c_1 = 0.45$; $c_2 = 1.95$; $c_3 = 0.20$ (thin solid line in **f**).

Fig. 13. Concrete beam modeled as a Timoshenko beam ($L/h = 10$, $\phi = 0.03$, $\alpha L = 3.65$) loaded by a counter-clockwise couple C acting at the midpoint and bonded to an orthotropic soil ($c_1 = 0.84$; $c_2 = 2.15$; $c_3 = 0.62$) in perfect adhesion (solid line) and in bilateral frictionless contact (dashed line). Dimensionless values of u_x (**a**), u_z (**b**), r_x (**c**), r_z (**d**), N (**e**), V (**f**), M (**g**) versus x/L . Horizontal displacement $u_{bx,0}$ (dash-dot line in **a**) refers to the centreline of the beam in perfect adhesion.

Table Captions

Tab. 1. Elastic moduli and Poisson's coefficients of the beams.

Tab. 2. Elastic moduli, Poisson's coefficients and c_i coefficients of the half-planes.

Tab. 3. GFRP Timoshenko beam ($L/h = 100$, $\alpha L = 106.4$, $\phi = 0.001$) subjected to a vertical force P_z at the midspan. Constant C and exponent λ of rate of convergence $C n_{eq}^{-\lambda}$ of the relative error for maximum bending moment e_M , using present analysis (PA) and two-dimensional FE models.

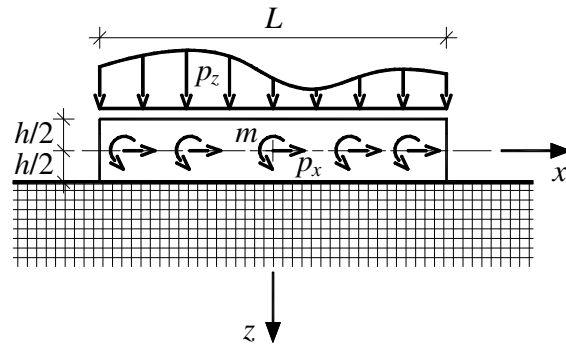


Fig. 1. Beam under general loads bonded to an orthotropic half-plane.

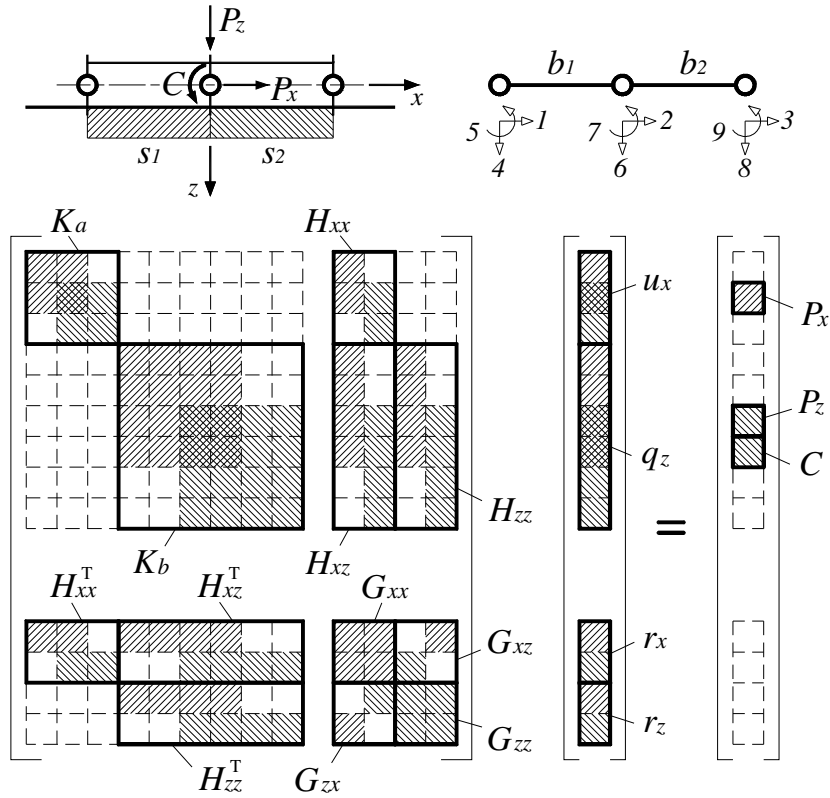


Fig. 2. Matrix system of a beam subdivided in two beam elements b_1 , b_2 , each of which is bonded to a single substrate element s_1 , s_2 , respectively. External pointwise loads P_x , P_z and couple C applied at the middle.

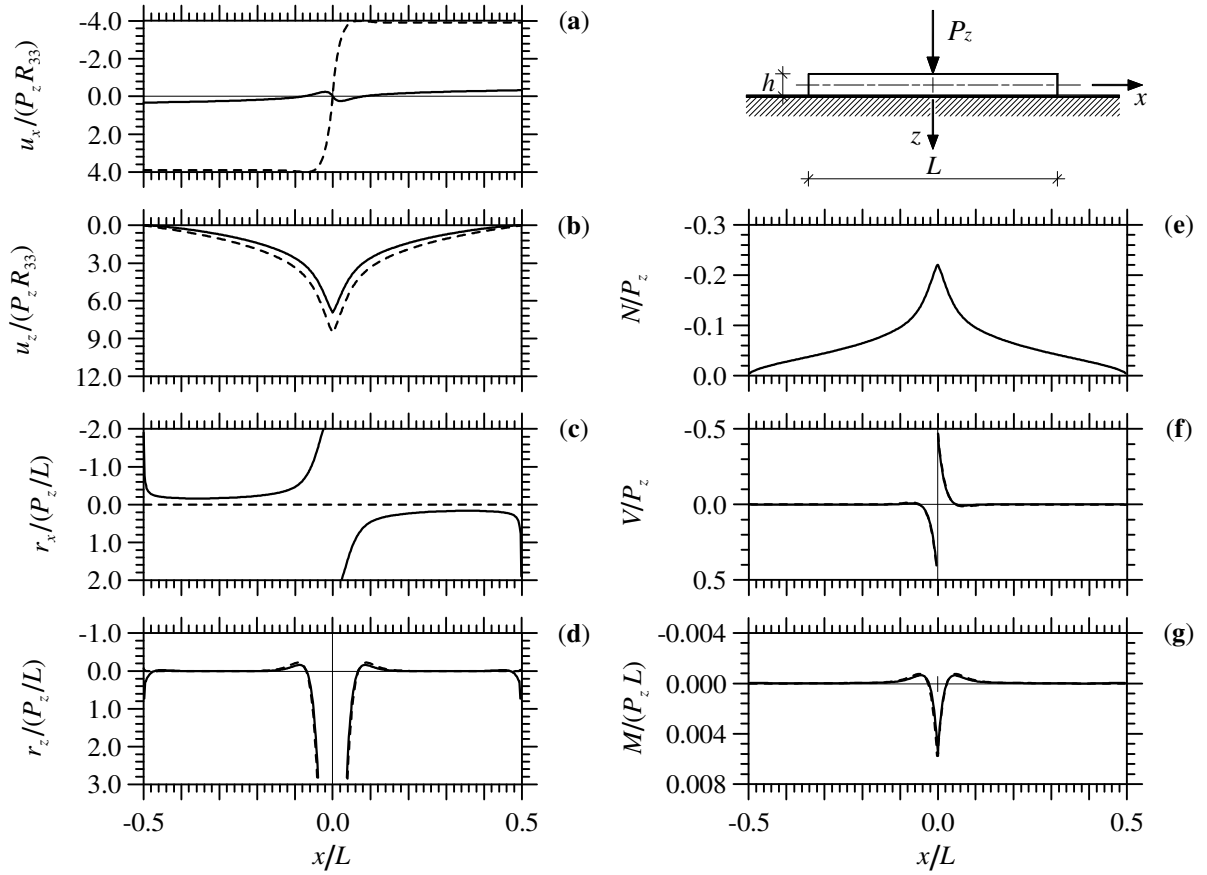


Fig. 3. GFRP Timoshenko beam ($L/h = 100$, $\alpha L = 106.4$ and $\phi = 0.001$) loaded by a vertical force P_z at the midpoint and bonded to a Balsa orthotropic half-plane in plane strain state ($c_1 = 2.91$; $c_2 = 2.24$; $c_3 = 7.81$) in perfect adhesion (solid line) and in frictionless contact (dashed line). Dimensionless values of u_x (a), u_z (b), r_x (c), r_z (d), N (e), V (f), M (g) versus x/L .

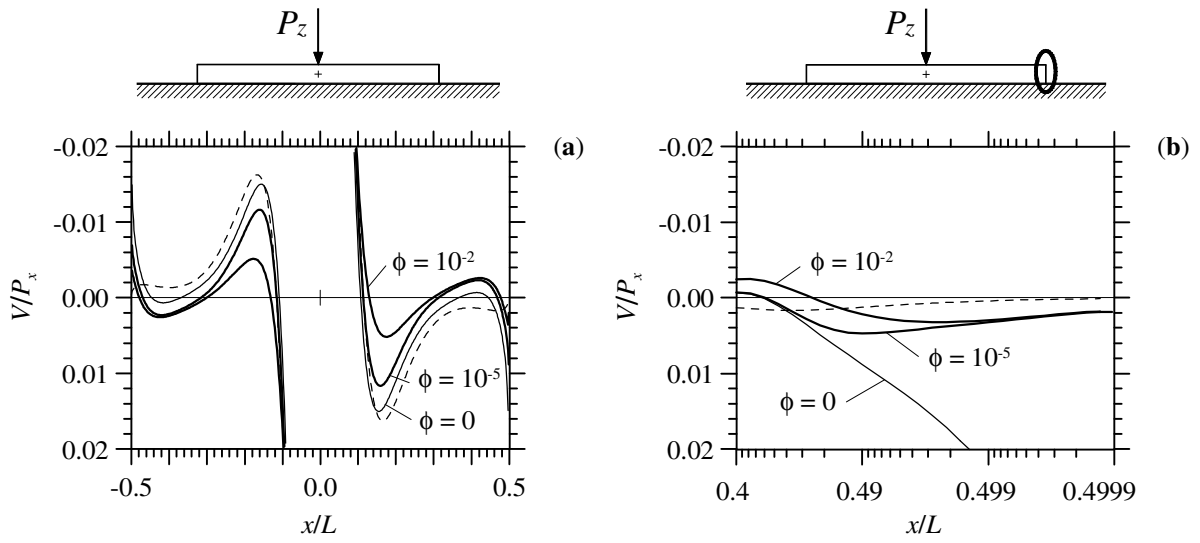


Fig. 4. GFRP Euler-Bernoulli ($\phi = 0$) and Timoshenko beams ($\phi = 10^{-2}$ and 10^{-5}) with $L/h = 40$ loaded by a vertical force P_z at the midpoint and bonded to Balsa orthotropic half-plane in plane strain state ($c_1 = 2.91$; $c_2 = 2.24$; $c_3 = 7.81$) in perfect adhesion $\alpha L = 42.5$ (solid line) and in frictionless contact for a GFRP Euler-Bernoulli beam ($\phi = 0$) (dashed line). Shear force V along the beam (a) and at the beam end (b).

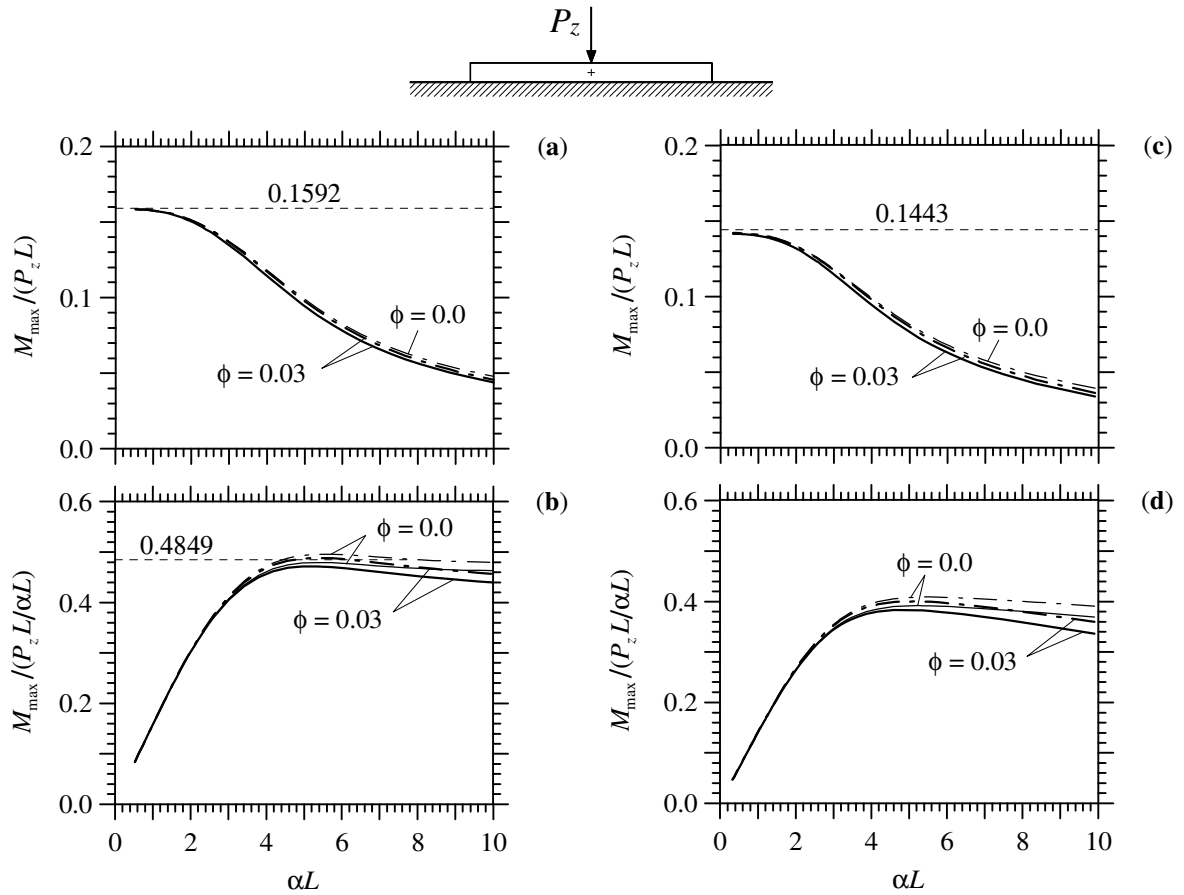
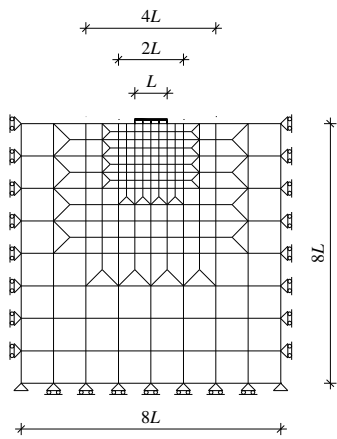
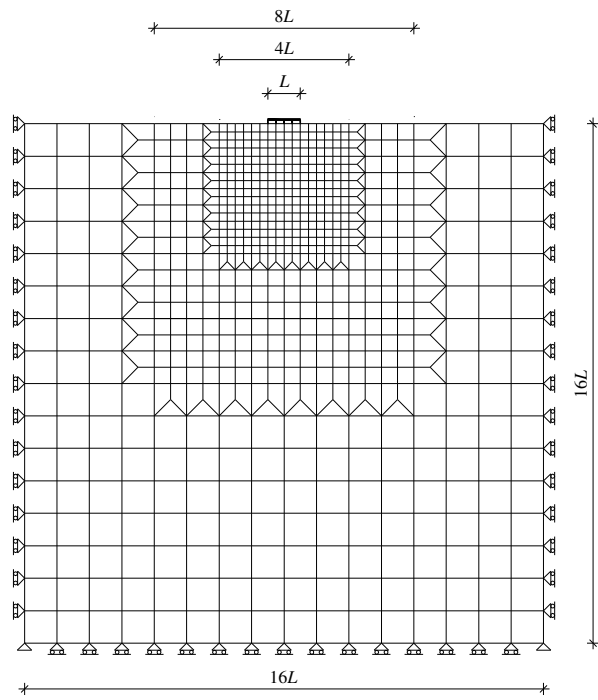


Fig. 5. Concrete beam loaded by a vertical force P_z at the midpoint, bonded to an orthotropic soil with $c_1 = 0.84$; $c_2 = 2.15$; $c_3 = 0.62$; $E_3 = 0.12\text{MPa}$ (solid line) and isotropic soil (dash-dot line). Bending moment M at the midspan versus αL of a beam in frictionless contact (a, b) and in perfect adhesion (c, d) for $\phi = 0.0$ and $\phi = 0.03$ (thin and thick line, respectively).



(a)



(b)

Fig. 6. Meshes adopted for the two-dimensional FE models with a beam subdivided into 4 equal FEs. Models with mesh dimension $8L$ (FEM $8L$) (a) and $16L$ (FEM $16L$) (b).

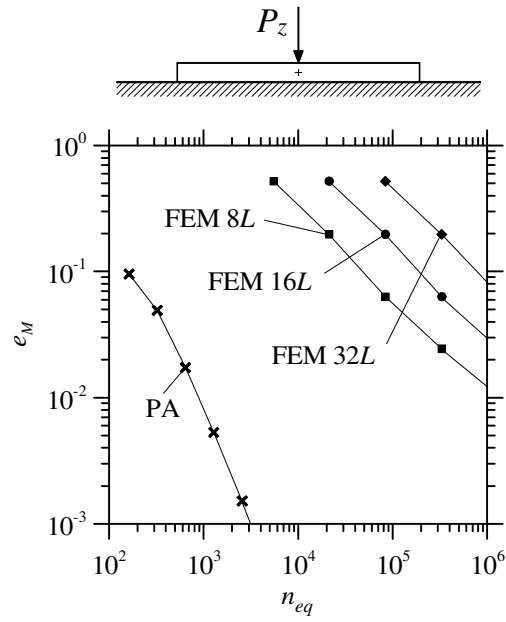


Fig. 7. GFRP Timoshenko beam ($L/h = 100$, $\alpha L = 106.4$, $\phi = 0.001$) loaded by a vertical force P_z at the midpoint and bonded to a Balsa orthotropic half-plane in plane strain ($c_1 = 2.91$; $c_2 = 2.24$; $c_3 = 7.81$). Relative errors of maximum bending moment $e_M = |M_{\max} - M_{\text{ref}}| / |M_{\text{ref}}|$ versus number of equations n_{eq} for the present analysis (PA) and for meshes FEM 8L, FEM 16L and FEM 32L.

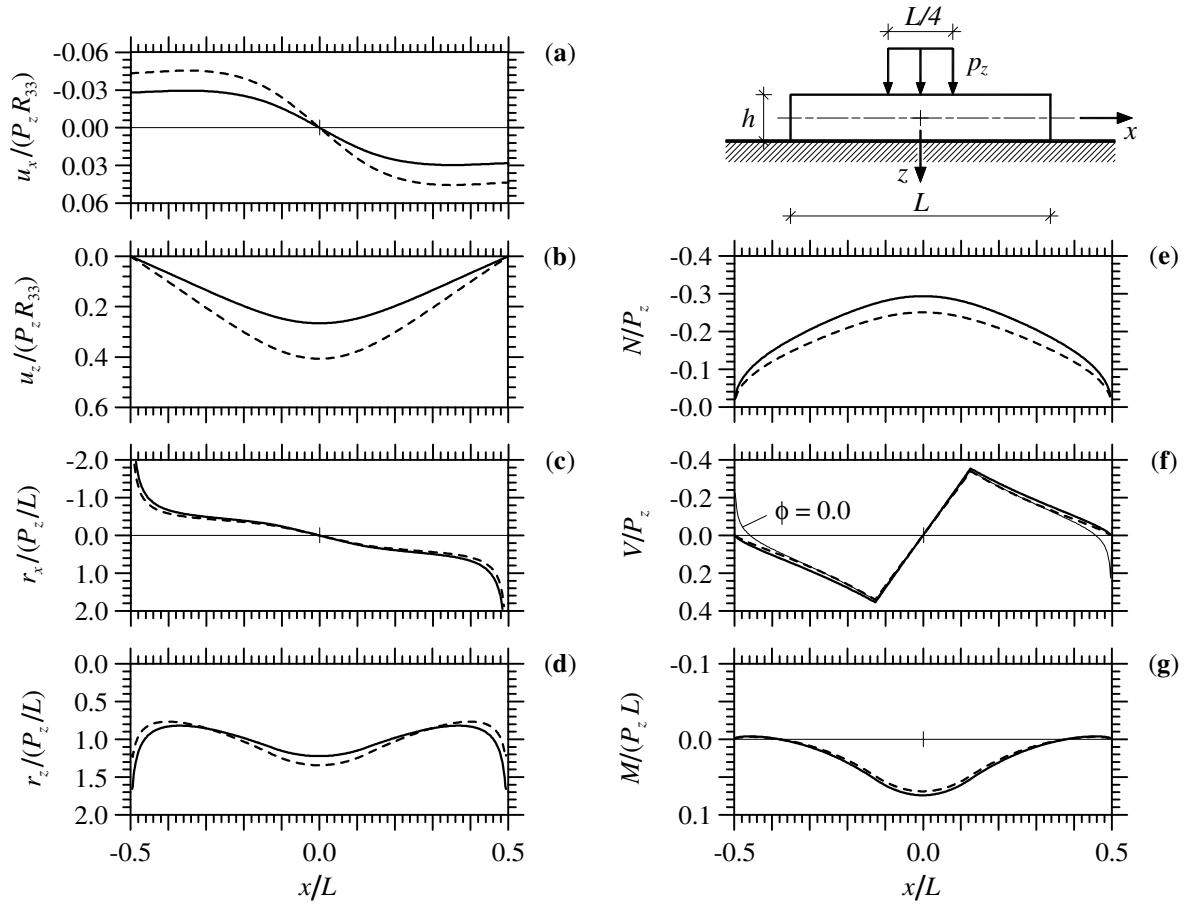


Fig. 8. Concrete beam subjected to an uniform vertical load distribution p_z acting over a length $L/4$ centered with respect to the midspan, resting on an orthotropic soil. Timoshenko beam ($L/h = 10$, $\phi = 0.03$) bonded to two kinds of orthotropic half-planes in perfect adhesion, $c_1 = 0.84$; $c_2 = 2.15$; $c_3 = 0.62$; $\alpha L = 3.65$ (solid line) and $c_1 = 1.06$; $c_2 = 2.15$; $c_3 = 0.93$; $\alpha L = 4.54$ (dashed line). Shear force V of an Euler-Bernoulli beam bonded to a half-plane with $c_1 = 0.84$; $c_2 = 2.15$; $c_3 = 0.62$; $\alpha L = 3.65$ (thin solid line in **f**).

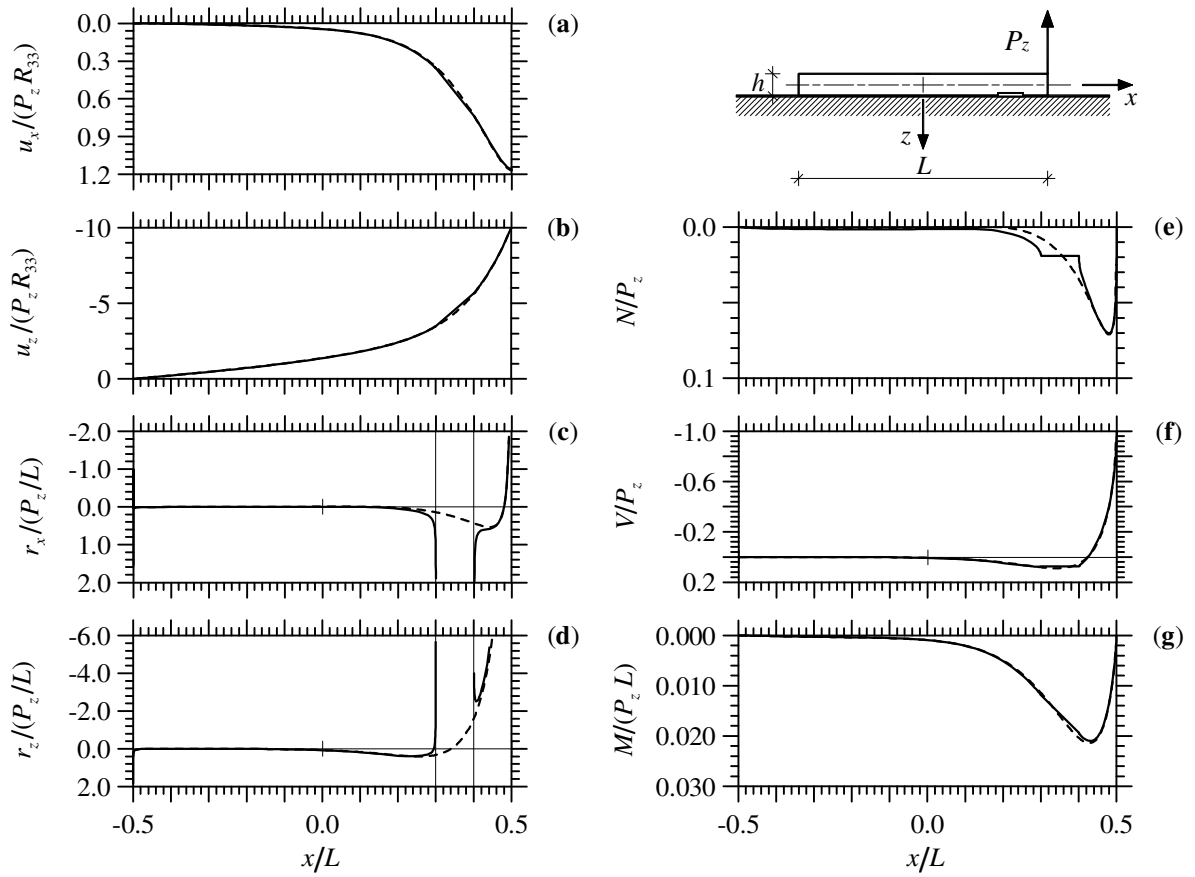


Fig. 9. GFRP Timoshenko beam ($L/h = 20$, $\alpha L = 21.3$ and $\phi = 0.02$) loaded by a vertical force P_z acting at a beam end and detached between $x/L=0.3$ and $x/L = 0.4$ (solid line) and perfectly bonded (dashed line) to Balsa orthotropic half-plane in plane strain state ($c_1 = 2.91$; $c_2 = 2.24$; $c_3 = 7.81$). Dimensionless values of u_x (a), u_z (b), r_x (c), r_z (d), N (e), V (f), M (g) versus x/L .

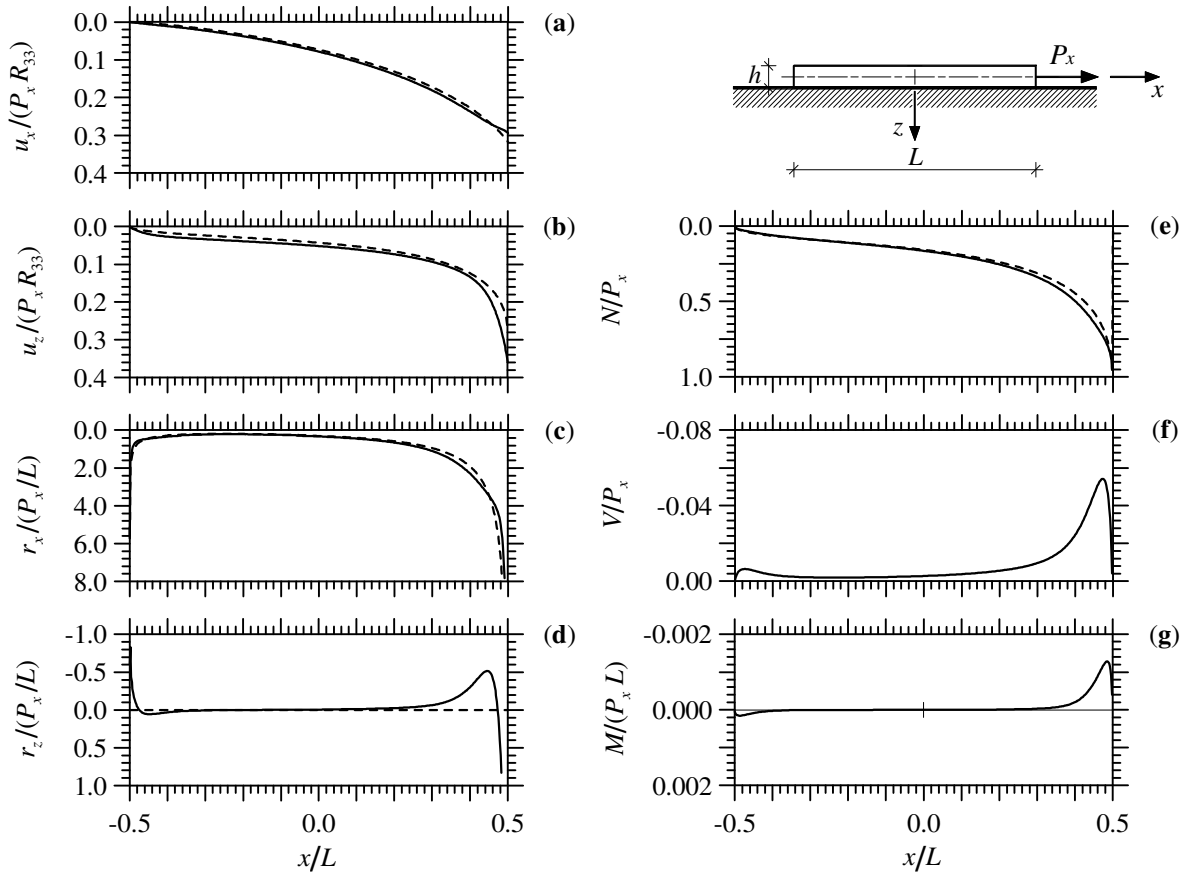


Fig. 10. GFRP Timoshenko beam ($L/h = 60$ and $\phi = 0.003$ with $c_1 = 0.70$; $c_2 = 2.40$; $c_3 = 0.44$) loaded by a horizontal force P_x acting at one end and bonded to a wood orthotropic half-plane in plane stress state ($c_1 = 0.56$; $c_2 = 2.22$; $c_3 = 0.28$) with $\alpha L = 40.2$ (solid line), and thin film assumption with $\beta L = 1.50$ (dashed line). Dimensionless values of u_x (a), u_z (b), r_x (c), r_z (d), N (e), V (f), M (g) versus x/L .

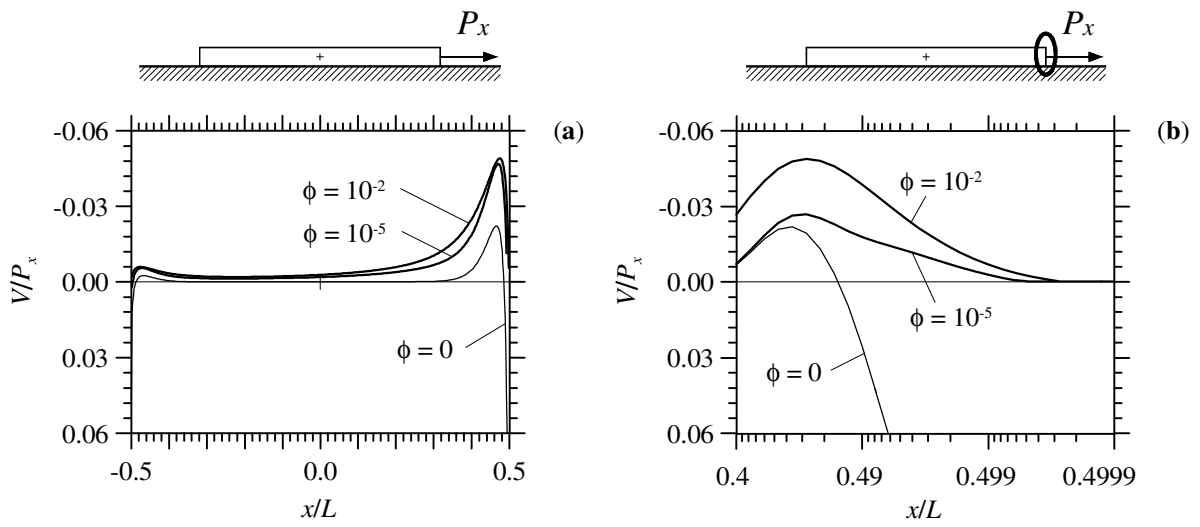


Fig. 11. GFRP Euler-Bernoulli ($\phi = 0$) and Timoshenko beams ($\phi = 10^{-2}$ and 10^{-5}) with $L/h = 60$ loaded by a horizontal force P_x acting at one end and bonded to a wood orthotropic half-plane in plane stress state ($c_1 = 0.56$; $c_2 = 2.22$; $c_3 = 0.28$) with $\alpha L = 40.2$. Shear force V along the beam (a) and at the beam end (b).

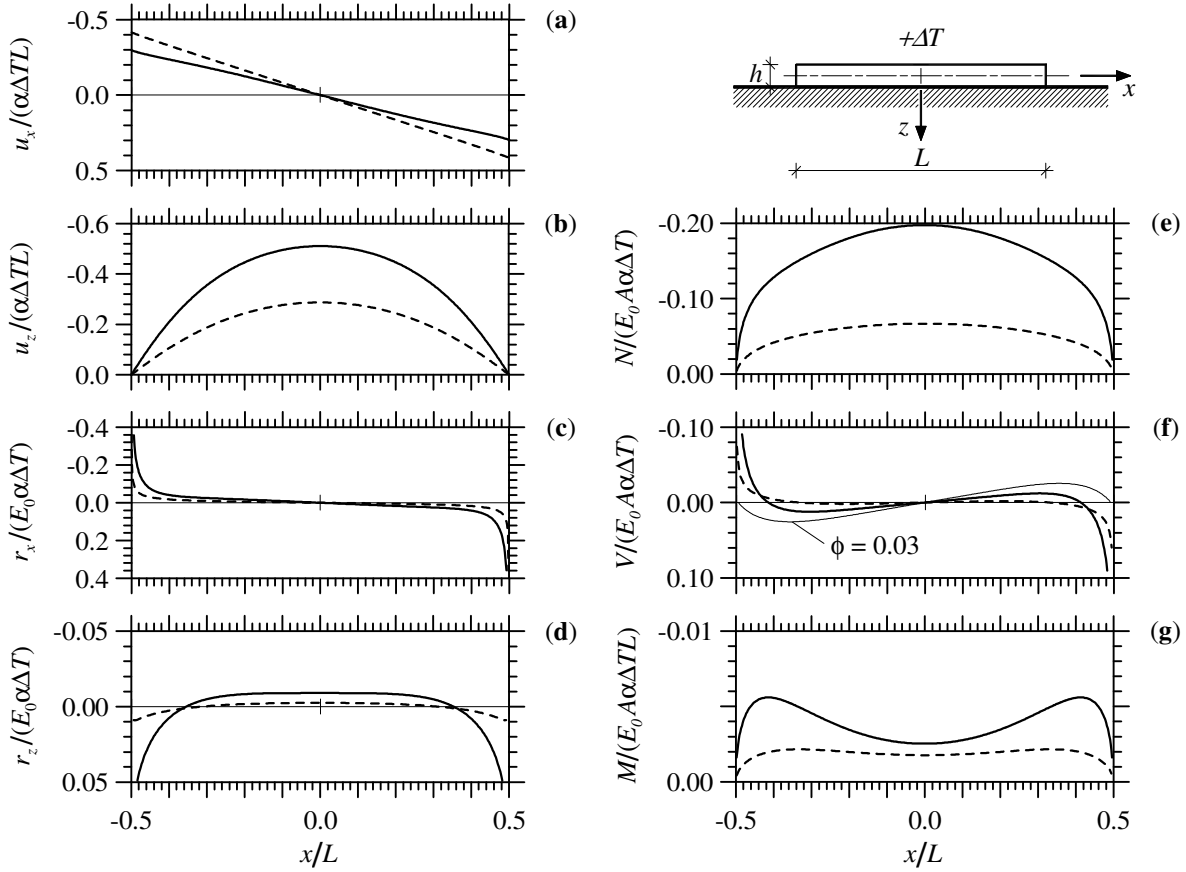


Fig. 12. Aluminium stiffener subjected to an uniform thermal variation $+\Delta T$ bonded to a wooden substrate. Euler-Bernoulli beam ($L/h = 10$, $\alpha L = 60$) resting on two kinds of orthotropic half-plane with $c_1 = 0.45$; $c_2 = 1.95$; $c_3 = 0.20$ (solid line) and $c_1 = 0.65$; $c_2 = 2.90$; $c_3 = 0.40$ (dashed line) in perfect adhesion. Dimensionless values of u_x (a), u_z (b), r_x (c), r_z (d), N (e), V (f), M (g) versus x/L . Shear force V of a Timoshenko beam ($\phi = 0.03$) bonded to half-plane with $c_1 = 0.45$; $c_2 = 1.95$; $c_3 = 0.20$ (thin solid line in f).

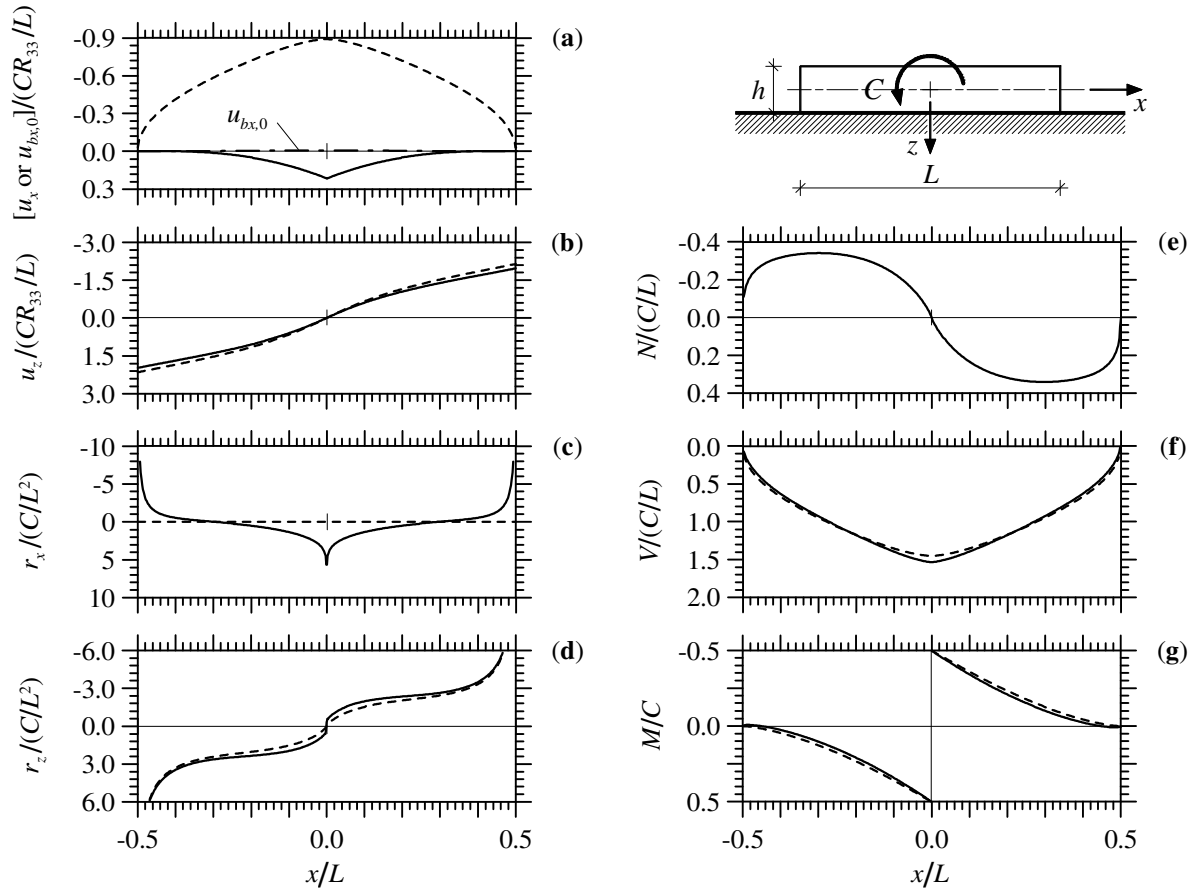


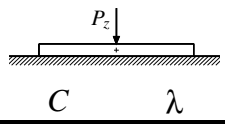
Fig. 13. Concrete beam modeled as a Timoshenko beam ($L/h = 10$, $\phi = 0.03$, $\alpha L = 3.65$) loaded by a counter-clockwise couple C acting at the midpoint and bonded to an orthotropic soil ($c_1 = 0.84$; $c_2 = 2.15$; $c_3 = 0.62$) in perfect adhesion (solid line) and in frictionless contact (dashed line). Dimensionless values of u_x (a), u_z (b), r_x (c), r_z (d), N (e), V (f), M (g) versus x/L . Horizontal displacement $u_{bx,0}$ (dash-dot line in a) refers to the centreline of the beam in perfect adhesion.

Beam	GFRP B1	Concrete B2	Aluminum B3
E_x [GPa]	40	30	70
E_z [GPa]	10	30	70
G_{xz} [GPa]	5	12	26
ν_{xz}	0.25	0.2	0.35

Tab. 1. Elastic moduli and Poisson's coefficients of the beams.

Substrate	Balsa	Clay	Sand	Wood		
	S1	S2	S3	S4	S5	S6
E_x [GPa]	0.05	0.24	0.18	10	24	5
E_z [GPa]	4	0.12	0.23	1	1	1
E_y [GPa]	0.2	0.24	0.18	-	-	-
G_{xz} [GPa]	0.15	0.06	0.07	1	2.7	0.3
ν_{xz}	0.006	0.14	0.12	0.35	0.06	0.12
ν_{xy}	0.165	0.18	0.19	-	-	-
ν_{yz}	0.012	0.15	0.12	-	-	-
c_1	2.91	0.84	1.06	0.56	0.45	0.65
c_2	2.24	2.15	2.15	2.22	1.95	2.9
c_3	7.81	0.62	0.93	0.28	0.2	0.4

Tab. 2. Elastic moduli, Poisson's coefficients and c_i coefficients of the half-planes.

GFRP – Balsa		
	C	λ
PA	837	1.70
FEM 8L	252	0.72
FEM 16L	925	0.75
FEM 32L	3072	0.76

Tab. 3. GFRP Timoshenko beam ($L/h = 100$, $\alpha L = 106.4$, $\phi = 0.001$) subjected to a vertical force P_z at the midspan. Constant C and exponent λ of rate of convergence $C n_{eq}^{-\lambda}$ of the relative error for maximum bending moment e_M , using present analysis (PA) and two-dimensional FE models.